THERMAL PROPERTIES OF URANIUM-MOLYBDENUM ALLOYS:

PHASE DECOMPOSITION EFFECTS OF HEAT TREATMENTS

A Thesis

by

JOHN THOMAS CREASY

Submitted to the Office of Graduate Studies of
Texas A&M University
in partial fulfillment of the requirements for the degree of

MASTER OF SCIENCE

December 2011

Major Subject: Nuclear Engineering

Thermal Properties of Uranium-Molybdenum Alloys: Phase Decomposition Effects of Heat Treatments

THERMAL PROPERTIES OF URANIUM-MOLYBDENUM ALLOYS:

PHASE DECOMPOSITION EFFECTS OF HEAT TREATMENTS

A Thesis

by

JOHN THOMAS CREASY

Submitted to the Office of Graduate Studies of
Texas A&M University
in partial fulfillment of the requirements for the degree of

MASTER OF SCIENCE

Approved by:

Co-Chairs of Committee,	Sean M. McDeavitt
	William Charlton
Committee Members,	Raymundo Arroyave
Head of Department,	Raymond Juzaitis

December 2011

Major Subject: Nuclear Engineering

ABSTRACT

Thermal Properties of Uranium Molybdenum Alloys: Phase Decomposition Effects of Heat Treatments. (December 2011)

John Thomas Creasy, B.S., Texas A&M University

Co-Chairs of Advisory Committee, Dr. Sean M. McDeavitt
Dr. William Charlton

Uranium-Molybdenum (U-Mo) alloys are of interest to the nuclear engineering community for their potential use as reactor fuel. The addition of molybdenum serves to stabilize the gamma phase of uranium, as well as increasing the melting point of the fuel. Thermal properties of U-Mo alloys have not been fully characterized, especially within the area of partial phase decomposition of the gamma phase of the alloy. Additional data was acquired through this research to expand the characterization data set for U-Mo alloys.

The U-Mo alloys used for this research were acquired from the Idaho National Laboratory and consisted of three alloys of nominal 7, 10, and 13 percent molybdenum by weight. The sample pins were formed by vacuum induction melt casting. Once the three sample pins were fabricated and sent to the Fuel Cycle and Materials Laboratory at Texas A&M University, the pins were homogenized and sectioned for heat treatment. Several heat treatments were performed on the samples to induce varying degrees of phase decomposition, and the samples were subsequently sectioned for phase verification and thermal analysis.

An Electron Probe Microanalyzer with wavelength dispersive spectroscopy was used to observe the phases in the samples as well as to characterize each phase. The density of each sample was determined using Archimedes method. Finally, a light flash analyzer was used to determine thermal diffusivity of the samples up to 300°C as well as to estimate the thermal conductivity. For U-10Mo, thermal diffusivity increased with increasing phase decomposition from gamma to alpha + U_2Mo while U-7Mo saw a flattening of the thermal diffusivity curve with increased phase decomposition.

DEDICATION

I dedicate this thesis to my family and friends, especially my grandparents Archie, Julia Virginia, and Eldridge. I also dedicate this thesis to Miranda, Dana, Dustin, Ashley, David, and Katie. Your memories will live on.

ACKNOWLEDGEMENTS

I would like to thank my committee chair, Dr. McDeavitt, and my committee members, Drs. Charlton and Arroyave, for their guidance and support throughout the course of my research.

I would like to thank my friends and colleagues and the Texas A&M Nuclear Engineering Department faculty and staff.

I would like to thank Drs. Wachs, Burkes, Staples, and Mr. Zocher for providing continuous guidance on this project and on life in general.

I would like to thank Chad Thompson, Grant Helmreich, Sandeep Irukuvarghula, Jeffrey Clemens, and Julie Borgmeyer for assistance and advice within the FCML. I am grateful for Drs. Guillemette and Popp for their assistance with the electron microprobe and X-Ray Diffraction (XRD).

I would like to thank Adam Shephard and Adam Hetzler for technical and editing assistance. I also want to extend my gratitude to the Idaho National Laboratory, which provided the test samples and experiment funding, and to the members of the Global Threat Reduction Initiative for providing motivation and funding.

Finally, I would like to extend a big thanks to my mother and father for their encouragement and love. I could not have done this without them.

NOMENCLATURE

at %	Atom Percent
DSC	Differential Scanning Calorimeter
EDS	Electron Dispersive Spectrometry
EPMA	Electron Microprobe Micro Analyzer
LFA	Laser/Light Flash Analysis
SEM	Scanning Electron Microscope
t	Time
U-Mo	Uranium Molybdenum Alloy
U-10Mo	Uranium with 10% Molybdenum by weight
wt %	Weight Percent
WDS	Wavelength Dispersive Spectrometry
XRD	X-Ray Diffraction

TABLE OF CONTENTS

Page

Page

Page

LIST OF FIGURES

Page

LIST OF TABLES

1. INTRODUCTION

Fuels with high quantities of fissile material per unit volume are desirable for several reactor situations, one of which is the high performance research reactor (HPRR). The material with the highest density of fissile uranium is uranium metal. Unfortunately, U metal is in most cases unacceptable as a reactor fuel due to undesirable properties that lead to fuel failure. This primarily arises as a consequence of the properties of the alpha (α) phase of U metal, which is the natural state of the metal below 660°C. The addition of one or more metals from Groups V through VIII have be found to increase the stability of uranium alloys [1]. One feature of these alloys is the stability of a body centered cubic solid solution crystal structure (gamma γ phase) that remains stable through a wide variety of temperature and fission rate conditions. A metal with a low neutron cross section from this group is molybdenum (Mo), which may be added in amounts of 5 to 20 at % to stabilize the alloy while still maintaining a high uranium density. Thus, Uranium-Molybdenum (U-Mo) alloys are a promising candidate for a fuel that has a balance of high fissile material density, and stable, predictable behavior.

It is a frequent practice to form fuel alloys by quenching the BCC γ phase to room temperature. While under irradiation, the uranium molybdenum (U-Mo) alloy fuels decompose from the solid solution γ phase into the α -U phase plus the U_2Mo intermetallic phase (also known as γ;' however, early literature referred to it at the δ phase). This new structure, which is the low temperature equilibrium structure, may lead

---

This thesis follows the style of the Journal of Nuclear Materials.

to irradiation induced tearing and higher incidences of fission gas release in the uranium fuel (leading to swelling and failure) since the grain structure of α-U and γ' are less geometrically consistent and ordered than the γ phase. Conversely, the fission events in the alloy can cause a recrystalization effect that acts to keep the material in the gamma phase [2, 3]. Larger quantities of molybdenum in the alloy generally increase the gamma stability of the fuel; quantities near the eutectoid concentration (~10 wt %) prove to be an ideal balance of stability and density. This makes U-Mo an interesting choice for applications such as new metallic reactor fuels that require a high fuel loading.

The properties of U-Mo alloys have been investigated with various levels of intensity since the 1950s when they were first employed as fuel for research reactors and critical assemblies in the U.S. and Russia [4]. More recently, The Reduced Enrichment for Research and Test Reactors (RERTR) program, currently the Global Threat Reduction Initiative (GTRI) Convert program, has been investigating U-Mo for several decades; this research serves as the foundation for the existing experiment. The GTRI Convert Fuel Development Program has chosen U-10Mo as the fuel alloy for the U.S. HPRRs. A series of screening tests were performed in which many alloys of uranium were irradiated to determine the best alloy for further testing. U-Mo alloys were found to be the top performers in the test series; research and development of this alloy for high density research reactor fuel then commenced. In 2008, U-10Mo was selected for the U.S. reactors, while many European reactors continued to pursue U-7Mo to achieve higher fuel densities.

The nominal fabrication process for U-Mo alloys is to cast and quench the material to stabilize the metastable gamma (γ) phase [5]. Casting in an inert gas is recommended to prevent the formation of oxides in the alloy. Rapid cooling is necessary to keep the alloy in the γ phase. A common technique used to accomplish this includes an homogenization step in which the alloy is brought to an elevated temperature between the eutectoid temperature (560°C) and the melting temperature for the alloy (1135°C to 1200°C). The alloy is held at temperature for an extended period of time to ensure the metal has completely transformed to the γ phase and to enable an even distribution of the molybdenum throughout the sample. The sample is then removed from the heat and quenched to lock the metal in the gamma metastable phase. Although metastable, the transformation/decomposition of γ phase U-Mo is extremely slow at room temperature. The U-Mo prepared in this fashion is referred to as γ stabilized [1]. The temperature and time durations necessary to induce the decomposition of γ stabilized U-Mo into combinations of α -U, β -U, γ, and γ' (U_2Mo) phases have been theoretically and experimentally determined [1, 6]; β-U is stable at very low Mo concentrations. An area of knowledge that requires further development is the quantification of the properties of U-Mo alloys with mixed phases after partial decomposition of the γ phase.

Thermal properties of U-Mo alloys with varying grain structure and composition have not been fully characterized; however, adequate characterization will enable more efficient design and fabrication of future fuel for reactors. The research described in this thesis provides new measurements of the thermal diffusivity up to 300°C for U-7Mo, U-

10Mo, and U-13Mo alloys in various stages of decomposition. Furthermore, the measurements are used to generate computational estimates of the alloys specific heat and thermal conductivity. Section 2 describes the technical background in which this thesis is based, including uranium metal alloy theory and properties. Section 3 describes the experimental design and procedures implemented in this research. Section 4 outlines the results achieved, and section 5 describes the importance and meaning of the results. Finally, section 6 briefly summarizes the primary findings and offers suggestions for future research.

2. BACKGROUND

2.1 Alloy Metallurgy and Structures

Uranium is naturally in the alpha phase at temperatures below 668°C, and this orthorhombic phase has low resistance to corrosion and oxidation, lacks dimensional stability and has a low yield strength [7]. It also reacts more readily with aluminum used in cladding and in dispersion fuels [8]. The isotropic and cubic (BCC) gamma phase of uranium has much better strength and ductility and lower susceptibility to corrosion and reactions with aluminum cladding; it cannot be retained in the gamma (metastable) phase without the addition of elements from groups V through VIII [1]. Molybdenum, along with zirconium, niobium, titanium, vanadium, chromium, rhenium and ruthenium, have been found to stabilize the gamma phase of uranium [9]. The most commonly used for alloying with U in a fuel applications are Mo, Zr, Nb, and Ti [8]. Molybdenum has a relatively large gamma phase region versus the other elements, and is found to be most promising for future research reactor fuels [7].

Uranium-Molybdenum may exist in several phases, and have been studied since the 1950's. The main phases of interest in the context of this thesis are the alpha, gamma, and U_2Mo (gamma prime). The beta phase only exists at molybdenum concentrations that are lower than those used in this experiment.

2.1.1 The Gamma (γ) Phase

The γ phase of uranium-molybdenum exists as a substitutional solid solution with an isotropic body centered cubic (BCC) crystal lattice. Above concentrations of 7 at%, U-Mo may be quenched to room temperature in the metastable gamma phase, or γ-stabilized phase. A metastable condition for a phase refers to the fact that it is not in its equilibrium state, as shown in a phase diagram. In this instance, the γ-stabilized phase may be retained indefinitely at temperatures below 300°C. This phase begins to decompose as the eutectoid temperature is approached, and the decomposition time is highly dependent on the molybdenum concentration [7]. The stable γ phase region exists from approximately 560°C to the liquidus temperature. The gamma phase unit cell parameter is [7]: a = 3.4409 Å.

2.1.2 The Alpha (α) Phase

The alpha phase of U-Mo is orthorhombic (See Fig. 2-1). Several versions of the alpha U-Mo phase can exist, with primarily a change in the "b" unit cell parameter, or deviation of the angle between "a" and "b" from 90 degrees[10]. Below approximately 560°C, an equilibrium U-Mo alloy above 6 wt% Mo is composed primarily of the alpha phase and U_2Mo (gamma prime) [9]. The unit cell parameters of U_2Mo are:

a = 2.869 Å , b = 5.709 Å , c = 4.962 Å .

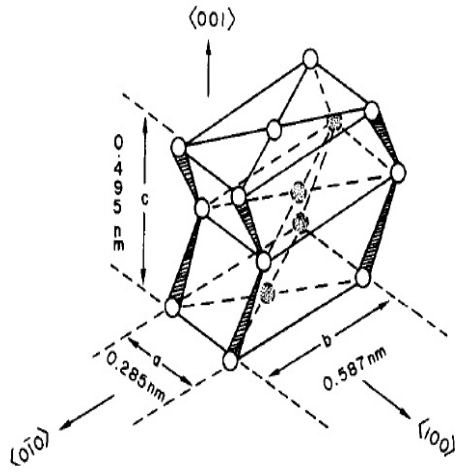

Figure 2-1: Alpha phase uranium[11].

2.1.3 The U_2Mo Phase (γ')

The intermetallic γ' phase is an ordered phase of U-Mo, and has a tetragonal form in which each Mo atom is surrounded by 8 U atoms, which arrange themselves in a closer spacing than the gamma phase[12]. The unit cell parameters of U_2Mo are: a = 3.427 Å , b = 9.834 Å , c/a = 2.871 Å .

2.1.4 The Beta Phase

Alloy compositions below ~7 at%, molybdenum (to the right side of the phase diagram shown in Fig. 2-2) are difficult to quench into the γ stabilized phase [7]. The beta phase of U-Mo is the primary phase formed during the decomposition from gamma to alpha phase in alloys containing less than 2 wt% Mo. A discussion of the beta phase properties is outside the scope of this investigation, but Yakel [11] and others have described the properties of this distorted tetragonal phase (Fig. 2-3).

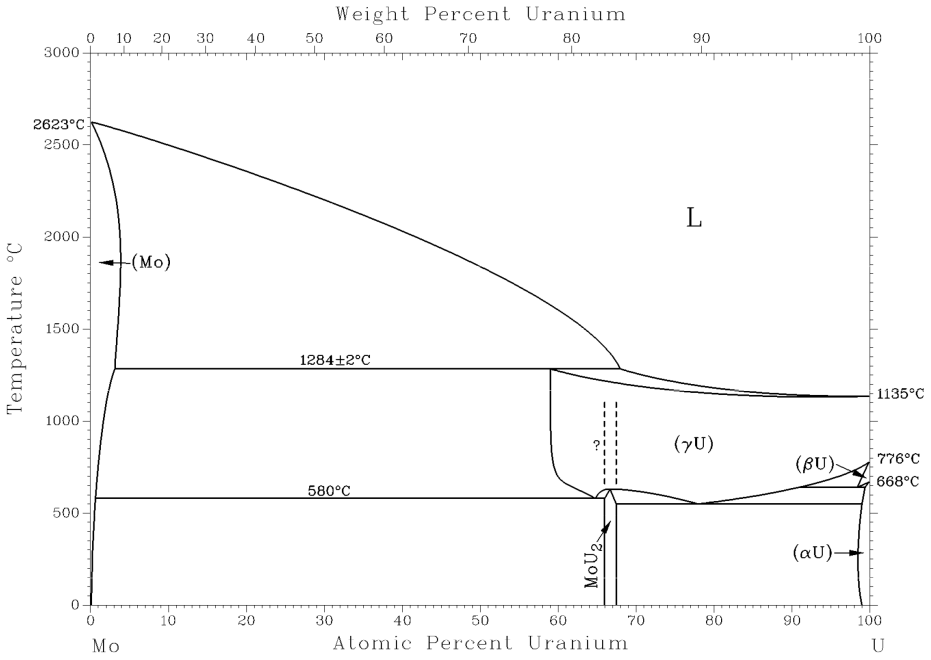

Figure 2-2: Uranium molybdenum phase diagram[13].

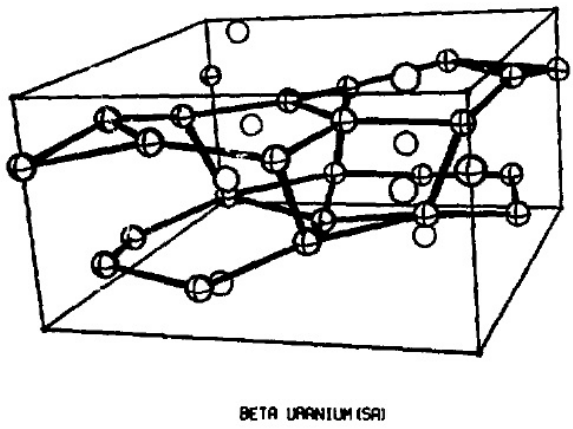

Figure 2-3: The beta phase of uranium.

2.1.5 Lattice Parameter

The lattice parameter of gamma phase U-Mo alloys is described in the following equation[13, 14].

$$a_0 = 3.4808 - 0.00314\, x_{Mo} \text{ Å} \tag{2-1}$$

where x_{Mo} is the Mo content in U-Mo alloy in atom %.

The lattice parameter, or lattice constant, is the constant, repeated distance between unit cells of a crystal lattice. The lattice parameter is completely defined by a set of three lengths and three angles which describe a unit parallelepiped. In the case of the γ U-Mo phase, which has a body centered cubic structure, only one parameter of the 6 is required. This is due to the fact that all angles are 90° and lengths are the same for a cube. Lengths given are typically in units of the angstrom. The lattice parameter is important because it defines the size of the repeatable structure in a metal's crystal lattice. From this value the density and behavior of the material in pure and mixed phases may be analyzed.

2.2 Phase Transformations

2.2.1 Phase Decomposition of U-Mo

The kinetics, structure, and timing of U-Mo alloy phase decomposition have been studied extensively. Rechtien and Nelson [10] observed the phases and distorted phases that occur during phase decomposition. The authors conducted numerous experiments involving uranium, plutonium, and neptunium, as well as alloys with other metals. In the

case of uranium, the temperature effects and phase change parameters were observed extensively. Observations relevant to this study include the methods of nucleation of new phases, the order of phase changes, and the identity of distorted phases in which lattice strain causes change in the length of the axes in the crystal structure. This observation also leads to some discussion on the dominance of shear on the phase decomposition during rapid cooling.

Howlett [15, 16] studied the decomposition of low at% U-Mo alloys and the phase structure of the results. The author presents a very detailed test matrix with observations of the phase change kinetics in low molybdenum alloys; the data include dilatometry measurements as well as XRD and microscopy. Procedures were described, and resultant TTT diagrams were also presented.

Ivanov and Virgiliev[17] observed the phase transformations of U-Mo with X-ray diffraction (XRD). The authors present a description of the gamma to U_2Mo phase decomposition, and their XRD results generate discussion of the precipitation method of U_2Mo in the lattice.

Several other authors [6, 18-20] expanded the knowledge base of the properties of U-Mo phase transformations. More specifically, Dwight[14], Burke[21] and Parida[7] detailed the martensitic transformation of gamma phase U-Mo to the alpha phase. Burke and Parida also detailed the distorted phases that occur during the phase decomposition.

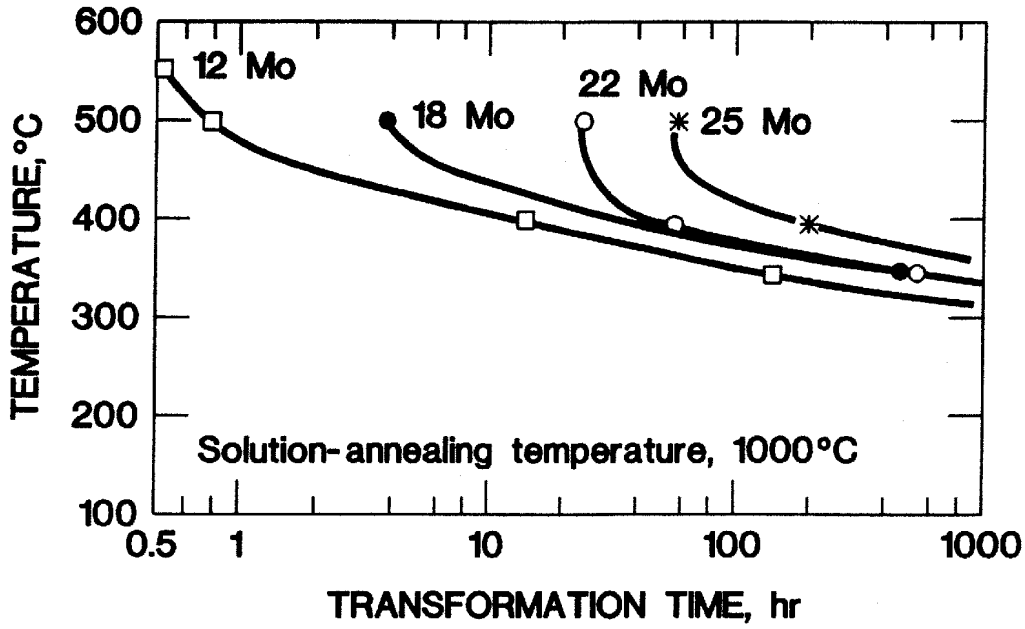

Figure 2-4: Time-temperature transformation diagram for U-Mo[11].

Figure 2-4 shows the time-temperature transformation (TtT) diagram for U-Mo. TtT diagrams are very valuable for phase decomposition studies due to their ability to visually convey the relationship between the isothermal temperature of a metal and the time scale upon which a phase change takes effect. For example, the line corresponding to 22 at% Mo is equivalent to U-10Mo, and from the figure, at 500°C, gamma phase decomposition begins at approximately 20 hours. 18 at% corresponds to approximately U-8Mo, and 25 at% refers to U-12Mo. For the alloys used in this present study, this diagram implies that the decomposition of the γ stabilized alloys of 8, 10, and 12 wt% should begin after ~4, ~21, and ~60 hours, respectively The tests alloys in this study

were nominally fabricated to be U-7Mo, U-10Mo, and U-13Mo (all wt %), but the actual measured concentrations were 8, 11, 14 wt% Mo, as discussed in Section 4.1.

2.2.2 Transformation of the Gamma Phase at Temperatures Near the Eutectoid

The eutectoid temperature of U-Mo exists near 10 wt% molybdenum. The eutectoid concentration corresponds to the most stable form of the gamma phase alloy. As a result, the gamma phase of the eutectoid concentration may exist at the lowest temperature before transformation/decomposition. As seen in Fig. 2-3, the eutectoid temperature is approximately 565°C.

The γ stabilized phase is attained by rapid cooling (quenching) of the γ phase from above the eutectoid temperature to a temperature well below the eutectoid. If the cooling rate is fast enough, the γ stabilized structure will remain indefinitely as a metastable phase at 25°C[14]. The onset of decomposition of the γ stabilized phase begins when the temperature approaches the eutectoid for the alloy (~565°C). A cellular decomposition begins in which lamellae nucleate from the grain boundaries of the gamma phase. These nuclei then grow to fill the grains and the reaction is controlled by grain boundary diffusion[19].

2.2.3 Fission Induced Recrystalization

The competing effects of phase decomposition versus fission induced recrystalization have been studied [2, 3] and research is underway to further characterize this phenomenon. This effect, while important in U-Mo reactor fuels, is not reproduced in this experiment. Fission induced recrystallization (FIC) occurs when the energy

released locally from fission acts to cause the reformation of the gamma phase in the fuel even though the material temperature is in a range in which decomposition of the gamma phase should occur.

Also of note is that low power metal fuel systems, such nuclear thermo-electric generators, may not be susceptible to the effects of FIC. This is notable because knowledge of the temperature induced phase transitions becomes more important when the phase of the metallic fuel is not maintained by fission effects.

2.3 Thermophysical Properties

2.3.1 Thermal Conductivity

Thermal conductivity (k) is a measure of a materials ability to conduct heat. For a one-dimensional treatment, it is defined as the quantity of thermal energy, ΔQ, transmitted during time Δt through a thickness x, in a direction normal to a surface of area A, due to a temperature difference ΔT, under steady state conditions and when the heat transfer is dependent only on the temperature gradient. More generally, it can be thought of as a flux of heat (energy per unit area per unit time) divided by a temperature gradient (temperature difference per unit length).

$$k = \frac{\Delta Q}{\Delta t}\frac{1}{A}\frac{\Delta x}{\Delta T} \tag{2-2}$$

$$k_{U-Mo} \approx 0.032T + 2.2 \quad \text{for } 298\text{ K} < T < 773\text{ K} \tag{2-3}$$

Here $K_{U\text{-}Mo}$ is in units of $W \cdot m^{-1}K^{-1}$ and T is absolute temperature. This equation applies to Molybdenum assays from 6-10 w% Mo.

Based on more recent literature, a correlation for the thermal conductivity was developed [11]. Please note that λ is synonymous with k.

$$\lambda_{U10Mo} = (.606 \pm 1.08) + (3.51 \times 10^{-2} \pm 1.61 \times 10^{-3}) \bullet T \tag{2-4}$$

This data is plotted in Fig. 2-5.

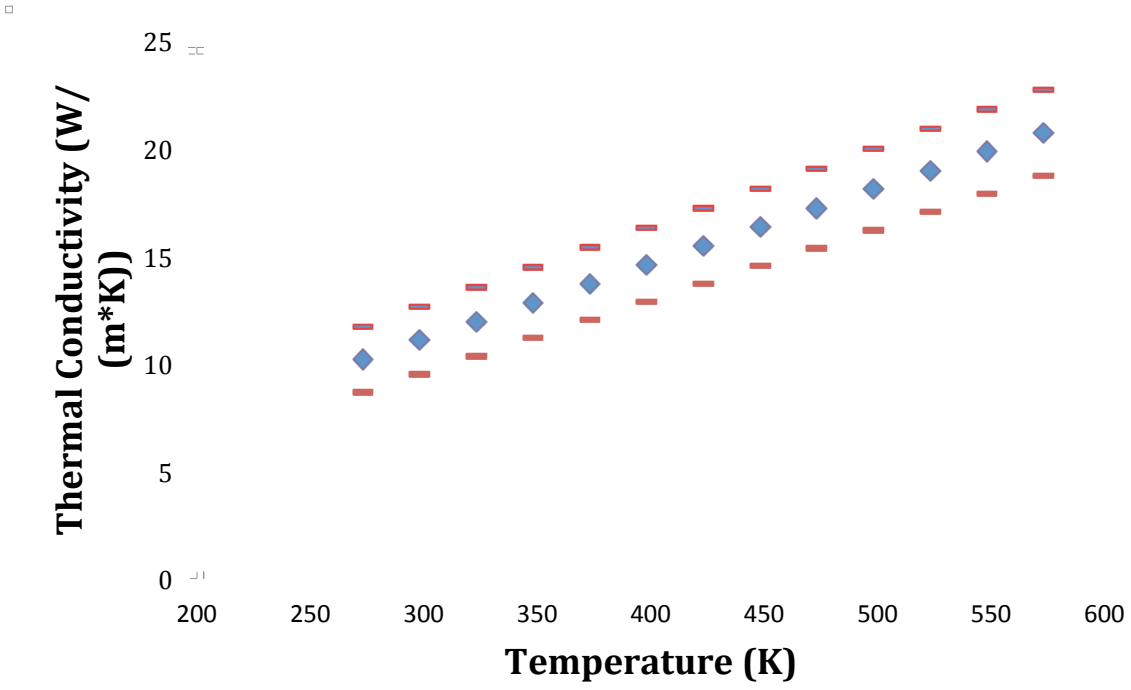

Figure 2-5: Thermal conductivity of U-10Mo [11].

Thermal conductivity of the alloy is important because changes in thermal conductivity in a reactor fuel may have undesirable effects on the entire reactor system.

Thermal conductivity also helps to define the specifications for the manufacturing method for the fuel.

It is useful to note that literature on thermal conductivity of gamma phase U-Mo alloys indicates that the thermal conductivity does not change significantly with relation to molybdenum content[8].

2.3.2 Thermal Diffusivity

Thermal diffusivity (α) is the ratio of thermal conductivity (k) to the volumetric heat capacity (ρC). It aids in describing a material's ability to attain thermal equilibrium with its surroundings.

$$\alpha = \frac{k}{\rho C} \tag{2-5}$$

Thermal diffusivity is related to the thermal conductivity of a material, as well as the density and specific heat capacity, as seen in the equation above.

While thermal diffusivity data has been published on U-Mo/Al dispersion fuels[22], only recently has it been published for metallic U-Mo[8], in which Burkes published the thermal diffusivity properties of gamma phase U-10Mo from approximately 200 C to 800 C. A study of the thermal diffusivity of U-Mo in the alpha and U2Mo phases has not yet been published.

2.3.3 Heat Capacity of U-Mo

Specific heat capacity (C_p) is the measure of the amount of thermal energy required to increase the temperature of a unit quantity of a material by a certain temperature interval.

$$Q = mC\Delta T \tag{2-5}$$

A recent correlation for C_p of U10Mo is given below in J/mol-K[13].

$$C_P^{UMo} = 29.84 - 8.90\times10^{-3}T + 4.32\times10^{-5}T^2 - 2.06\times10^{-8}T^3 \tag{2-6}$$

Table 2-1: Specific (molar) heat capacity of U-10Mo alloy.

Temperature, °C	Heat Capacity, J/mol-K
0	30.1
100	31.7
200	33.3
300	35.0
400	36.7
500	38.3
600	40.0
700	41.7
800	43.2
900	44.9
1000	46.6

From Burkes[8], the most recent correlation for the C_p of gamma phase U-10Mo is:

$$C_{P,U-10Mo} = (0.113\times10^3 \pm 4.28) + (7.05\times10^{-2} \pm 5.20\times10^{-3})\bullet T \tag{2-7}$$

where C_p is given in units of J/kg-K.

Heat capacity of U-Mo is important because it can have effects on the performance of the fuel in reactor as well as the manufacturing technique. See Table 2-1 for measured values of specific heat capacity.

Parida[7] created a correlation for U-8Mo (see equation below), and did so utilizing a Calvet calorimeter. A calvet calorimeter is one that uses a ring of thermocouples surrounding the sample to determine the total heat transfer into or out of the sample area. This results in a near complete integration of the heat in three dimensions and allows for increased sample sizes with high accuracy.

$$C_{p.m}(\frac{J}{K \bullet mol}) = 20.8 + 1.174 \times 10^{-2} \bullet T(K) + \frac{.4715 \times 10^5}{T^2} \tag{2-8}$$

where C_p refers to the specific heat at constant pressure, and T is the temperature in Kelvin.

Burkes[8] recently published correlations for U-10Mo, using a differential scanning calorimeter (DSC), and related the data to similar literature, as well as the Kopp-Neumann rule, which states that a good estimate of a mixture's specific heat capacity is the sum of the heat capacities multiplied by the mass fractions.

$$C = \sum_{i=1}^{N} (C_i \cdot f_i) \tag{2-9}$$

2.3.4 Density Calculations

Uranium Molybdenum alloy in the gamma phase has a density approximated by the following equation:

$$\rho_{U-Mo} = X_{Mo}\rho_{Mo} + (1 - X_{Mo})\rho_U \tag{2-10}$$

This approximation should be treated as an upper bound for the density of U-Mo alloys, as effects such as impurities and porosity lead to lower values. See Table 2-2 for measured values of the density and melting point of U-Mo.

Table 2-2**:** Density and melting point of U-Mo alloys.

Density and Melting Point		
Of Gamma-Stabilized Uranium Alloys		
	Density	**Melting**
Alloy Wt. %	**g/cm3**	**Point (C)**
U	19.0	1135
U-2Mo	18.5	1135
U-5Mo	17.9	1135
U-6.5Mo	17.5	1135
U-8Mo	17.3	1135
U-9Mo	17.0	1160

2.4 X-Ray Diffraction (XRD) Spectra of U-Mo

X-ray diffraction (XRD) is the standard method for determining phase/crystal composition in metals. In this investigation it was used to verify the phase composition of the various alloys following heat treatments. Relative peak heights are used to estimate the percent composition of each phase. For the gamma stabilized alloys, only the peaks for gamma phase U-Mo are expected. These are present at 2-theta angles of 36.6º, 52.6º, and 63º[23]. In the fully gamma decomposed samples little to no gamma phase material is expected to remain, and instead the peaks of the alpha phase (35º,

35.6º, 39.5º, 51º, and 60.3º) and U_2Mo (delta phase) (insert angles) are expected. An example of U-7Mo with strong gamma peaks is given in Figure 2-6.

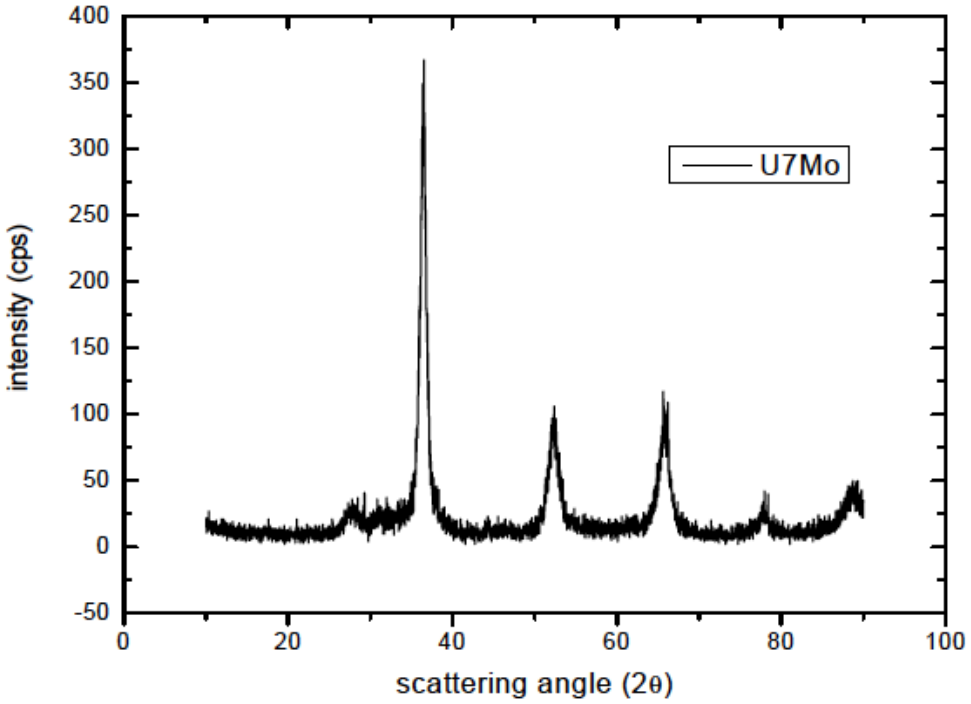

Figure 2-6: U-7Mo with primarily gamma phase peaks[23].

Halteman [12], Ivanov [17], Yakel [11] and more recently, Oliveira [23], Keiser [24], and Burkes [8], have utilized X-ray diffraction (XRD) to explore and characterize U-Mo alloy phases, and later to confirm the phase(s) present in the material. Halteman characterized U_2Mo in 1956, and utilized heat treatment techniques to decompose U-15Mo, and subsequently characterize the crystal structure using XRD. Ivanov et al. examined the structure of gamma phase decomposition of several uranium alloys. The

authors use XRD techniques to investigate the decomposition of gamma uranium into the alpha and U_2Mo phases. In particular the authors describe the mechanisms by which the alpha phase heterogeneously precipitates as particles in the matrix, followed by a homogenous decomposition of the remainder of the gamma phase material into the U_2Mo phase as well as the alpha particles. In researching fuel types to replace HEU with LEU in research reactors, Keiser, Burkes, and Oliveira used XRD to determine the phase composition of their samples for dispersion and monolithic fuel applications. Dispersion fuel is uranium-based material (U-Al_X for example) dispersed as particles in the meat of the fuel plates. Monolithic fuel refers to a solid continuous “slab” of uranium metal alloy that makes up the fuel meat within the cladding.

3. EXPERIMENTAL DESIGN AND PROCEDURES

This section describes the experimental methods, equipment, and procedures used to carry out the fabrication and characterization of the U-7Mo, U-10Mo, and U-13Mo alloys. Section 3.1 descries the methods used to fabricate U-Mo pins as well as the methods used to homogenize, quench, and prepare samples for characterization. Section 3.2 describes the subsequent methods used to characterize the alloys.

3.1 Alloy Fabrication, Heat Treatment, and Sample Preparation

3.1.1 Metal and Pin Casting

Three Uranium Molybdenum alloys were cast at the Idaho National Laboratory at the FASB facility in the Materials and Fuels Center (MFC). Depleted uranium metal feedstock (<0.21 wt.% 235U, 99.8% purity) and molybdenum foil (Alfa Aesar, 99.95% purity) were charged into a Centorr Model 5SA single arc furnace. The alloyed ingot was melted three times to achieve adequate homogenization, and the ingot was turned over prior to each melt. The ingot was then melted and cast into a 12.5mm diameter by 60mm cylindrical hollows in a graphite mold. Three different molybdenum concentrations were created with nominal concentrations of 7 wt % (16 at %), 10 wt % (21.5 at %) , and 13 wt % (37 at %). The U-13Mo pin is shown in Figure 3-1 following unpackaging and the Texas A&M FCML.

Figure 3-1: Photograph of the cast U-13Mo pin received from Idaho National Laboratory; 0.5 inch diameter by 2 inch length.

3.1.2 Homogenization and Quenching Procedures

The cast U-Mo pins from INL were sealed in stainless steel tubes in and argon atmosphere (see Figure 3-2). The tubes and end caps (Swagelok) were made of Type 304 stainless steel. Within the capsule the pins were wrapped in tantalum foil to prevent interactions between the steel and the uranium. Copper slugs were placed in either end of the SS tube to aid in heat conduction during quenching. The samples were then heated to 900°C for 52 hours to guarantee homogenization as noted in literature. After the heat treatment, the encapsulated alloys were removed from the furnace and quenched in 0°C

water. The cooling time was found to be adequately estimated by bulk analysis, and a uniform temperature of below 300°C was found to be attained in less than 4 minutes.

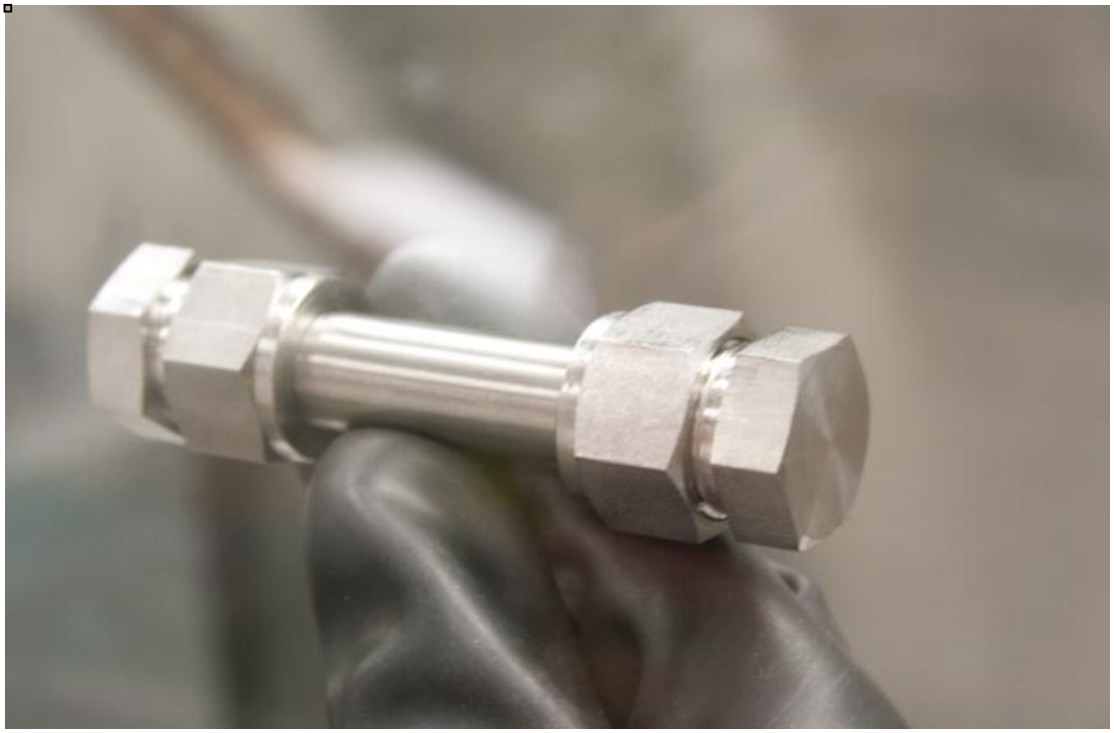

Figure 3-2: U-Mo sample encapsulated.

Figure 3-3: Sectioned U-Mo sample after homogenization and quenching.

3.1.3 Sectioning for Heat Treatment

A diamond saw within a fume hood was used to cut the 2 inch long pins into thirds for heat treatments, as seen in Figures 3-3 and 3-4. Cutting time varied with blade sharpness and molybdenum assay, and ranged from 5 minutes to up to 2 hours per cut. Oil lubrication was used to prevent rapid oxidation of the particulate U-Mo resulting from the cutting. Samples were ultrasonically cleaned in an ethanol-water mixture following cutting to prevent contamination.

Figure 3-4: Diamond saw in fume hood.

3.1.4 Heat Treatment Development

Following the homogenization process to ensure the U-Mo is quenched in the γ phase, controlled decomposition of this phase into the α and U_2Mo phase may be performed by heating the material to just below the U-Mo eutectoid temperature (565°C). The rate of decomposition generally accelerates as the eutectoid temperature is approached.

The onset of decomposition of the gamma phase of Uranium-Molybdenum can be described by the following decay equation[19]:

$$t = Ae^{\frac{-Q}{RT}} \tag{3-1}$$

In the above equation t represents time until onset of phase decomposition, A is a constant, Q is the activation energy of transformation, R is the gas constant, and T is the temperature in K. In Fig. 3-5, values taken from TtT diagrams in literature [refs] were used to create an approximation for the onset of gamma phase decomposition with respect to the weight percent content of molybdenum.

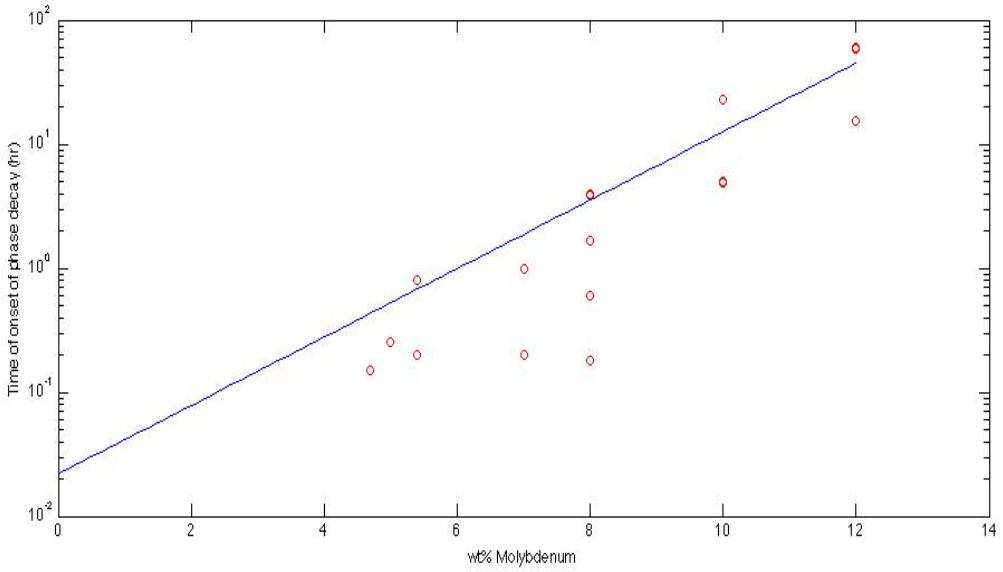

Figure 3-5: Time until onset of gamma phase decomposition.

The percent decay of the gamma phase may also be approximately related to the time at isothermal temperature by the Avrami equation.

$$Y = 1 - e^{(-kt^n)} \tag{3-2}$$

where k and n are time independent constants. The constant *n* is related to the methods for nucleation and directions of growth [25]. For U-Mo, the γ to α + γ' transformation

nucleates at grain boundaries, and then proceeds to grow into the grains [19]. This indicates that $n<3$ [25]. Rearranging the equation for known values of phase decay and time allows for determination of the value of *k.* Once *k* is known, the amount of phase decomposition may be predicted for a given time at temperature (isothermal 500C for this case). For U-Mo, it is assumed that the constant *n* will be similar to U-Nb, U-Zr, and U-Nb-Zr in that *n* at early time intervals is high (n=3), and at longer time intervals is much smaller (n<2)[26]. Grain size also appears to influence the value of *n* and samples of identical composition and heat treatment can have different transformation rates if grain sizes are significantly different. This is apparent when a calculation of the surface area in the sample occupied by the grains is made. Smaller grains equate to larger surface area occupied by grain boundaries, and since grain boundaries are the nucleation site for this alloy, the reaction will occur sooner and faster.

A prediction was created for the start and end of phase decomposition at 500°C for varying weight percent values of molybdenum. Values were taken from historical literature. Most literature only contained the start of decomposition time, while few detailed the completion time.

In Fig. 3-6, the data from literature is plotted and exponential line of best fit is rendered across the data set. In Fig. 3-7, a more detailed algorithm was used in Matlab to approximate the best fit to the data.

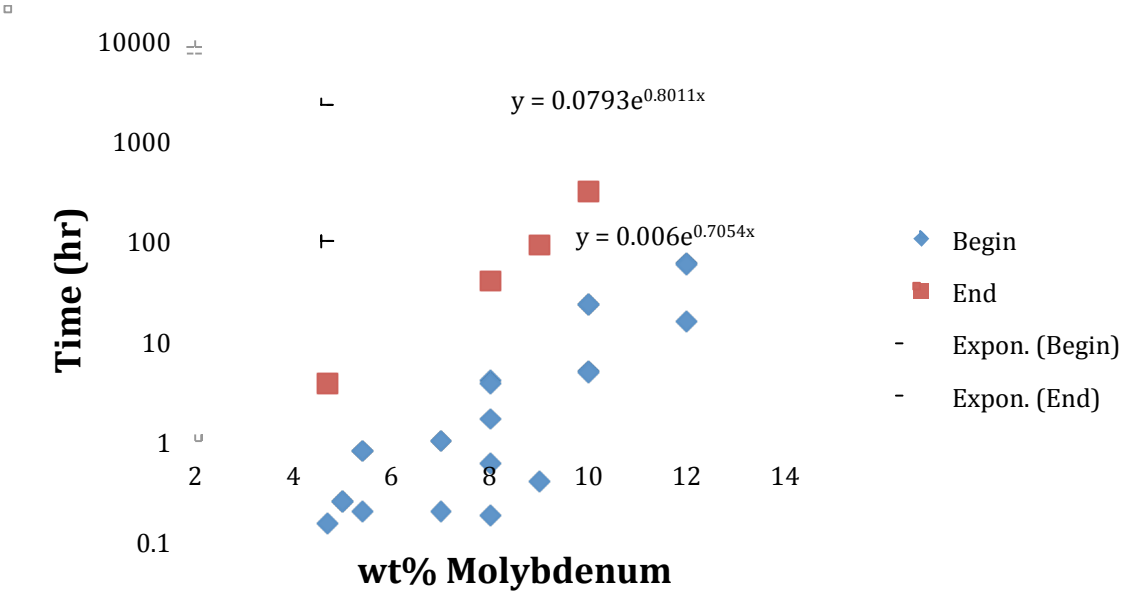

Figure 3-6. Start and completion time for phase decomposition with respect to molybdenum concentration.

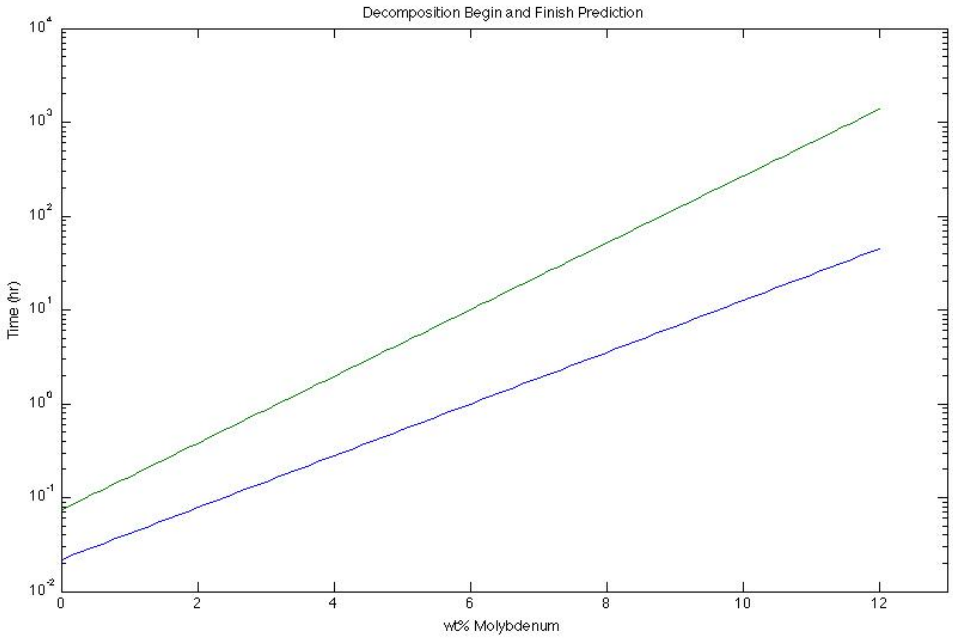

Figure 3-7: Detailed approximation of start and finish times for U-Mo decomposition at 500 C with respect to molybdenum concentration.

For Fig. 3-7 above, the equation for the start of decomposition was determined to be:

$$T = .0219e^{.653X} \tag{3-2}$$

where T is the time to start transformation and X is the wt% molybdenum.

Heat treatments were performed using a furnace well inside of an argon atmosphere glove box. Table 3-1 below shows the series of heat treatments performed in this experiment. The first two heat treatments were planned, where all of the samples needed to be initially γ stabilized, and a 96 hour heat treatment at 500°C was estimated to result in some decomposition for all of the samples. Following a more in-depth literature review and analysis of historical data, heat treatments 3 and 4 were planned to more accurately cover the range of phase decomposition for each sample. In Table 3-1, heat treatment 4 could not be completed for U-10Mo and U-13Mo, as situations occurred to prevent the completion of these long duration treatments. For U-13Mo, a time of 200 hours of the 360 desired was reached, while the U-10Mo 200 hour duration sample was not able to be heat treated. All heat treatments were conducted at 500°C. Heat treatments were conducted in argon atmosphere furnaces both within an inert atmosphere glovebox and tube furnaces with flowing argon to prevent oxidation.

Table 3-1: U-Mo test matrix.

	Heat Treat 1	**Heat Treat 2**	**Heat Treat 3**	**Heat Treat 4**
U7Mo	homogenized gamma	96 hours	5 hours	14 hours
U10Mo	homogenized gamma	96 hours	40 hours	200 hours*
U13Mo	homogenized gamma	96 hours	166 hours	360 hours*

3.2 Alloy Characterization Methods

3.2.1 Density Measurement

The density of each sample was measured using the Archimedes principle, which states, “an object immersed in a fluid is buoyed up by a force equal to the weight of the fluid displaced by the object.” Using this principle, the following equation can be used to find the density of an object.

$$\frac{density\ of object}{density\ of\ fluid} = \frac{weight\ of\ object}{(weight\ of\ object) - (measured\ weight\ of\ object\ in\ fluid)} \qquad (3\text{-}3)$$

The process for determining the density of the samples was accomplished using the apparatus in Fig. 3-8 and the following procedure:

1. Measure the mass of the sample
2. Remove sample from balance (Mettler, Model AL204),
3. Place container of fluid on the scale, with its weight supported so that it does not register on the scale,
4. Place sample holding “trapeze” on the scale, with sample holder suspended in the fluid. The mass of this “trapeze” should register on the scale
5. Tare the mass of the sample holder,
6. Place the U-Mo sample in the basket of the “trapeze,” while verifying that:
    a. The sample is covered entirely by the fluid and,
    b. The basket of the “trapeze” is not in contact with the side of the fluid container,

7. Measure the mass of the immersed sample,
8. Calculate the density of the sample using the equation above

This method may be used for any material that is more dense than the fluid in which it is immersed.

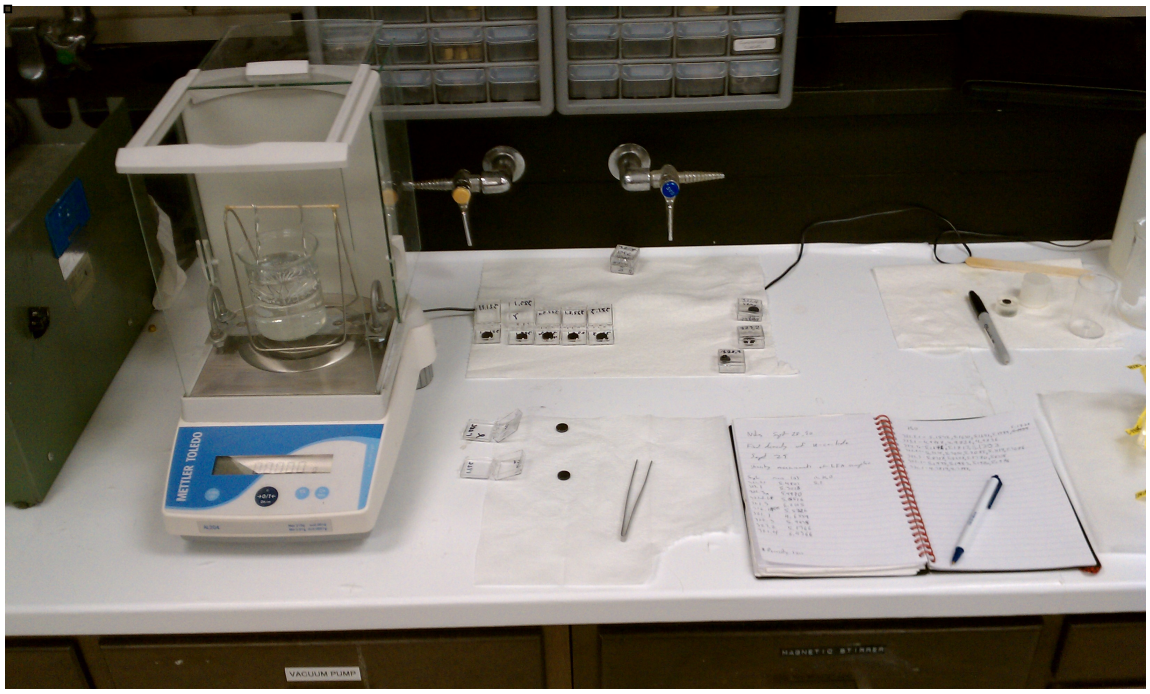

Figure 3-8: Setup for measuring sample density.

3.2.2 Microscopy

Electron Probe Micro-Analysis (EPMA) samples were prepared by casting a thin slice of the U-Mo sample into epoxy resin, then rough sanding to 400 grit by hand. This was followed by sanding to 1200 grit on a Minimet polisher. Final polish to ¼ micron diamond suspension in oil was then completed by hand. A carbon sputter coater was

used to apply a conductive coating of carbon to the surface of the polished U-Mo samples. This served a double purpose in that is helped retard the oxidation of the sample when being transported from inert gas environment to the EPMA.

A Cameca SX50 EPMA was used for the backscatter electron imaging (BSE) and wavelength dispersive spectroscopy (WDS) of the samples. The sample holder, including reference standards as well as two U-Mo samples are shown in Fig. 3-9, and the microprobe is shown in Fig. 3-10.

For the backscatter electron (BSE) images of the samples, Photoshop CS4 and Image SXM (based on Image NIH) were used to process and quantify the images. Contrast was raised in the images, and thresholding was used to count the percent area of the image composed of uranium carbide, γ phase U-Mo, and α + U_2Mo areas. Then a noise reduction algorithm was used to smooth the image, and the process was repeated for each sample.

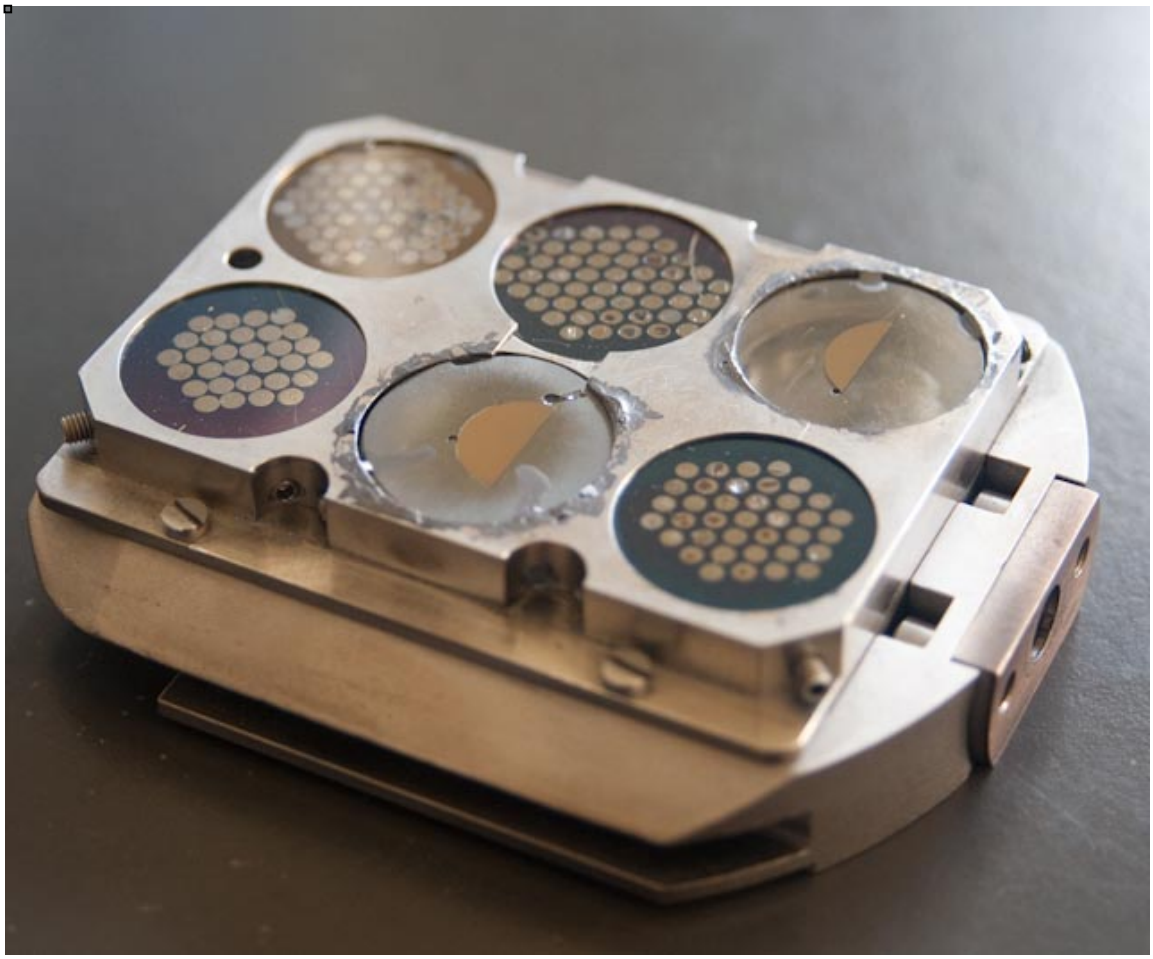

Figure 3-9: U-Mo samples loaded for insertion into the EPMA.

Figure 3-10: Cameca SX50 EPMA.

Images from the EPMA were analyzed using Image SXM (version of Image NIH), and Photoshop CS4. Thresholding was used to determine the percentage of the sample composed of each phase, and the quantity of particles and pits.

To quantify the composition of the light and dark regions of the images, wavelength dispersive spectrometry (WDS) was used. This technique counts the x-rays of a specific wavelength after they are diffracted through a crystal in the EPMA to isolate the x-rays of interest. This allows for accurate characterization of the material of interest in the microprobe.

3.2.3 Phase Composition Analysis with X-ray Diffraction (XRD)

An X-ray diffractometer was used along with EPMA to conduct the phase analysis. For the XRD runs, the samples to be used for the LFA were cleaned ultrasonically with ethanol to remove any remaining graphite from their surface, then surfaced with 280 grit sandpaper.

3.2.4 Thermal Properties Analysis with Light Flash Analyzer (LFA)

Thermal diffusivity of the samples was determined by Light/Laser Flash Analysis (LFA) using a Netzsch LFA 447 and Proteus analytic software package, as shown in Fig. 3-11.

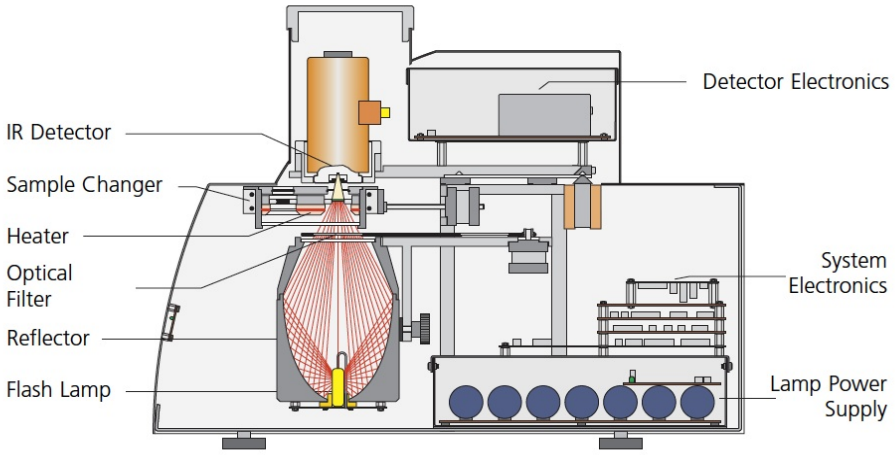

Figure 3-11: Nanoflash LFA 447 (Courtesy of Netzsch).

In this experiment the following methodology is used for the LFA:

- The controlling computer is used to set up a test matrix, which varies the furnace temperature and recording parameters for the experiment. The test matrix is designed to determine the thermal diffusivity of the sample at point along a range of temperatures
- The furnace is then used to bring the sample holder and samples to the initial temperature set by the test matrix.
- The laser/light bulb is fired and a predetermined amount of thermal energy is imparted to one side of the sample
- The detector is activated and records the energy/temperature of the opposing side of the sample versus time. This will allow for the computer/user to determine the speed at which thermal energy diffuses through the sample

- The sample is brought back to the test temperature (its temperature will rise due to the energy from the light/laser) and the process is repeated several times to attain statistically significant data
- The furnace is then used to take the sample to the next temperature in the test matrix, and the process is repeated
- Once the data has been collected for all points on the test matrix, the data is then processed via software to determine the thermal diffusivity. This software bases its initial estimate on the "half time method"[27], shown below.

$$a = 0.1388 \bullet \frac{d^2}{t^{\frac{1}{2}}} \tag{3-4}$$

The software also takes into account factors such as radial and surface heat losses [27].

4. RESULTS

This section provides the results from this project. Section 4.1 describes the density measurements for all samples. Sections 4.2 through 4.4 provide comprehensive results summaries for each alloy (U-7Mo, U-10Mo, and U-13Mo, respectively).

4.1 Alloy Density Measurements

The measured densities of the samples were slightly lower than estimated theoretical density for each alloy. This may be due to porosity, impurities, and slightly higher than nominal molybdenum concentrations. The density of the as-cast samples compared to the homogenized and heat treated samples are presented in Table 4-1. Large samples were measured early in the experiment, and the smaller samples were measured later during the course of the investigation. The first column of Table 4-1 gives the sample identifier as well as the average for each alloy type. The second column gives the measured density determined with Archimedes principle. The third column gives the estimated density determined by dimensional analysis, and the fourth column gives the theoretical density for each alloy type.

Table 4-1: U-Mo density measurements.

Sample	Measured Density (g/cm^2)	Est. Density (g/cm^2)	Theoretical (g/cm^2)
321 Large avg.	17.16		17.71
321.1	16.85	16.88	
321.2	16.99	17.05	
321.3	16.74	17.27	
321.4	16.94	17.01	
322 Large avg.	16.82		17.2
322.1	16.49	16.72	
322.2	16.59	16.58	
322.3	16.62	16.49	
323 Large avg.	16.51		16.72
323.1	16.15		
323.2	16.16		
323.3	TBD		

It was determined by EPMA analysis that the molybdenum concentrations in each of the cast samples were about one percent higher than originally reported. Therefore, the alloys on hand may be better approximated as U-8Mo, U-11Mo, and U-14Mo, but the original labels will be used throughout the rest of this document for clarity. The higher Mo content is consistent with the lower density measurements in Table 4-1.

4.2 U-10Mo Sample Results

4.2.1 U-10Mo XRD Results

Sample 322.1, which was U-10Mo gamma stabilized, showed only the gamma phase present, while samples 322.2 and 322.3 (U-10Mo at 96 and 40 hours, respectively), showed the presence of alpha + U_2Mo. The XRD results are displayed below in Table 4-2.

Table 4-2: XRD results for U-10Mo.

U-10Mo	Time @ 500 C	Phases Present
Heat Treat 1	Quench	gamma
Heat Treat 2	96 hours	alpha, U2Mo, gamma
Heat Treat 3	40 hours	alpha, U2Mo, gamma

4.2.2 Microscopy Results

Energy Dispersive Spectroscopy (EDS)

For initial qualitative determination of the elemental composition of areas of interest in the EPMA. In Fig. 4-1 below, EDS was used to verify that the dark particles present in all of the samples (see Figs. 4-2 to 4-4) were in fact uranium carbide. Note that the dark particle spectrum in Fig. 4-1 lacks molybdenum and has a higher carbon content.

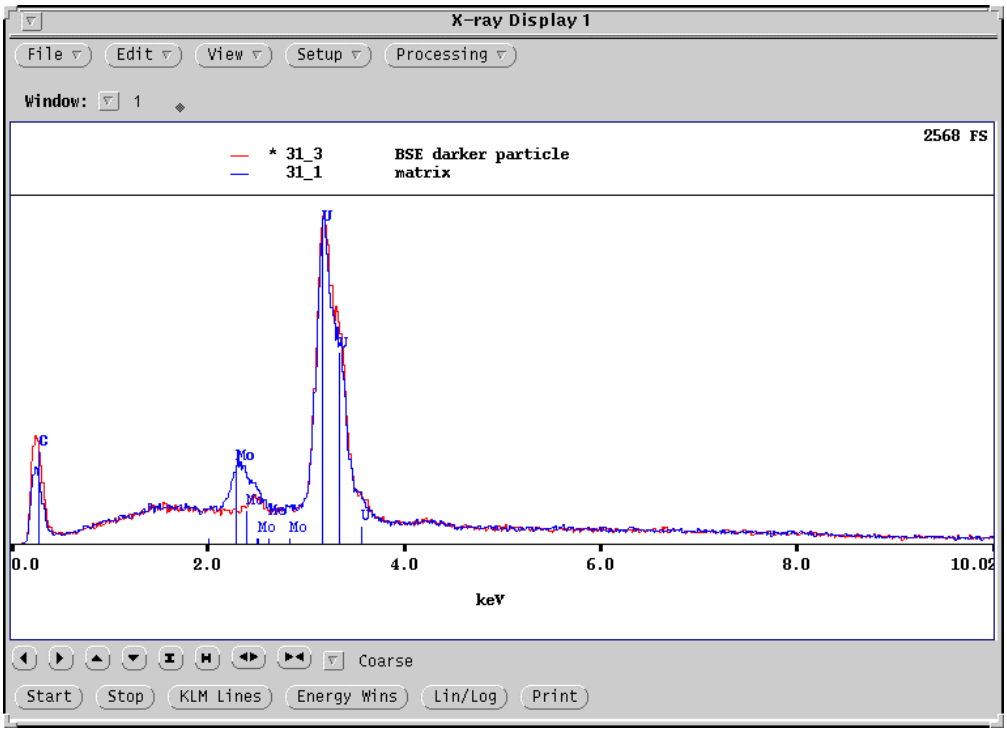

Figure 4-1: Superposition of sample matrix EDS with uranium carbide EDS.

The images taken at 200X magnification are presented in the following pages. The remainder of the images may be found in Appendix A.

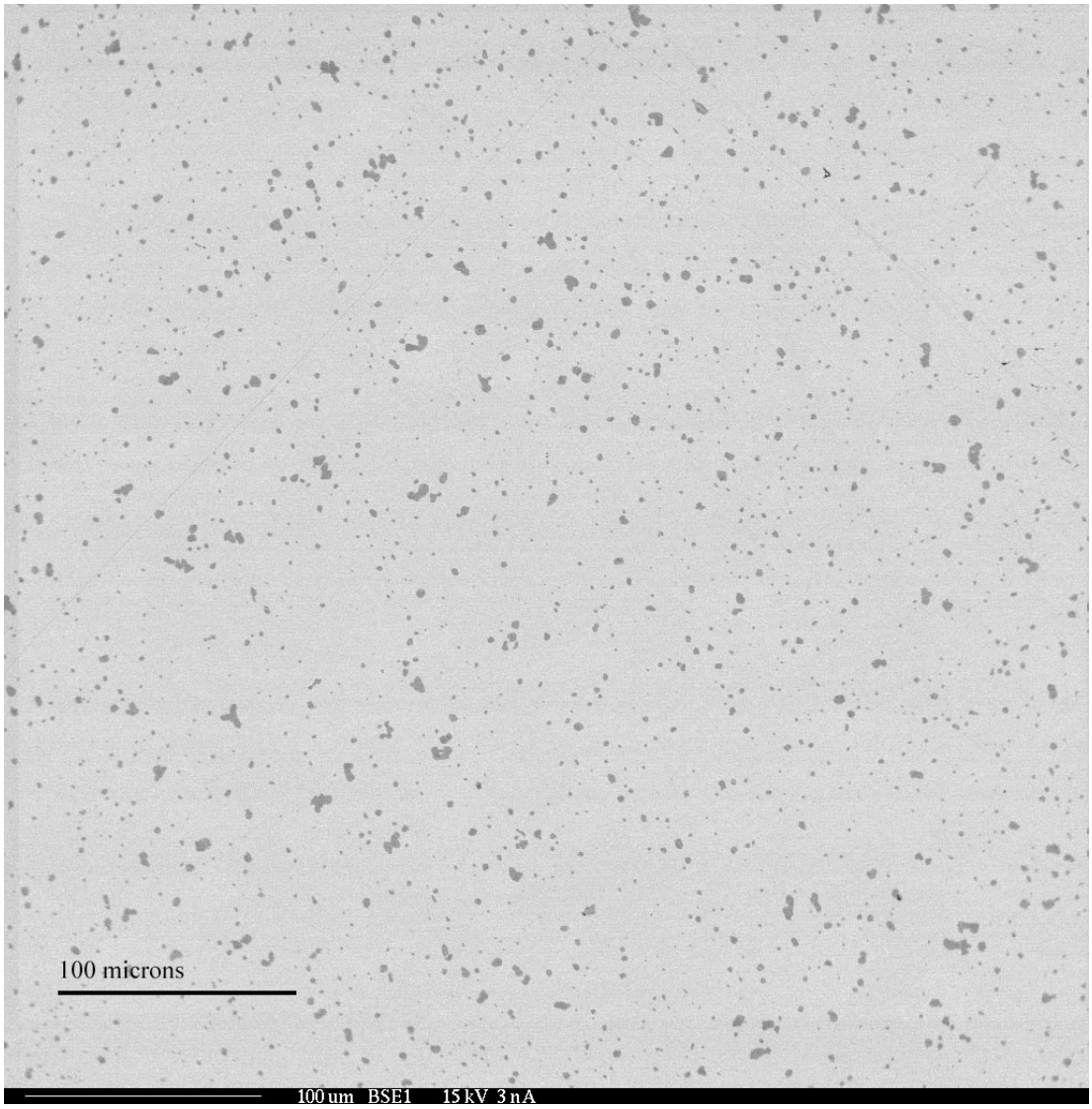

Figure 4-2: Sample 3221, U-10Mo in gamma phase.

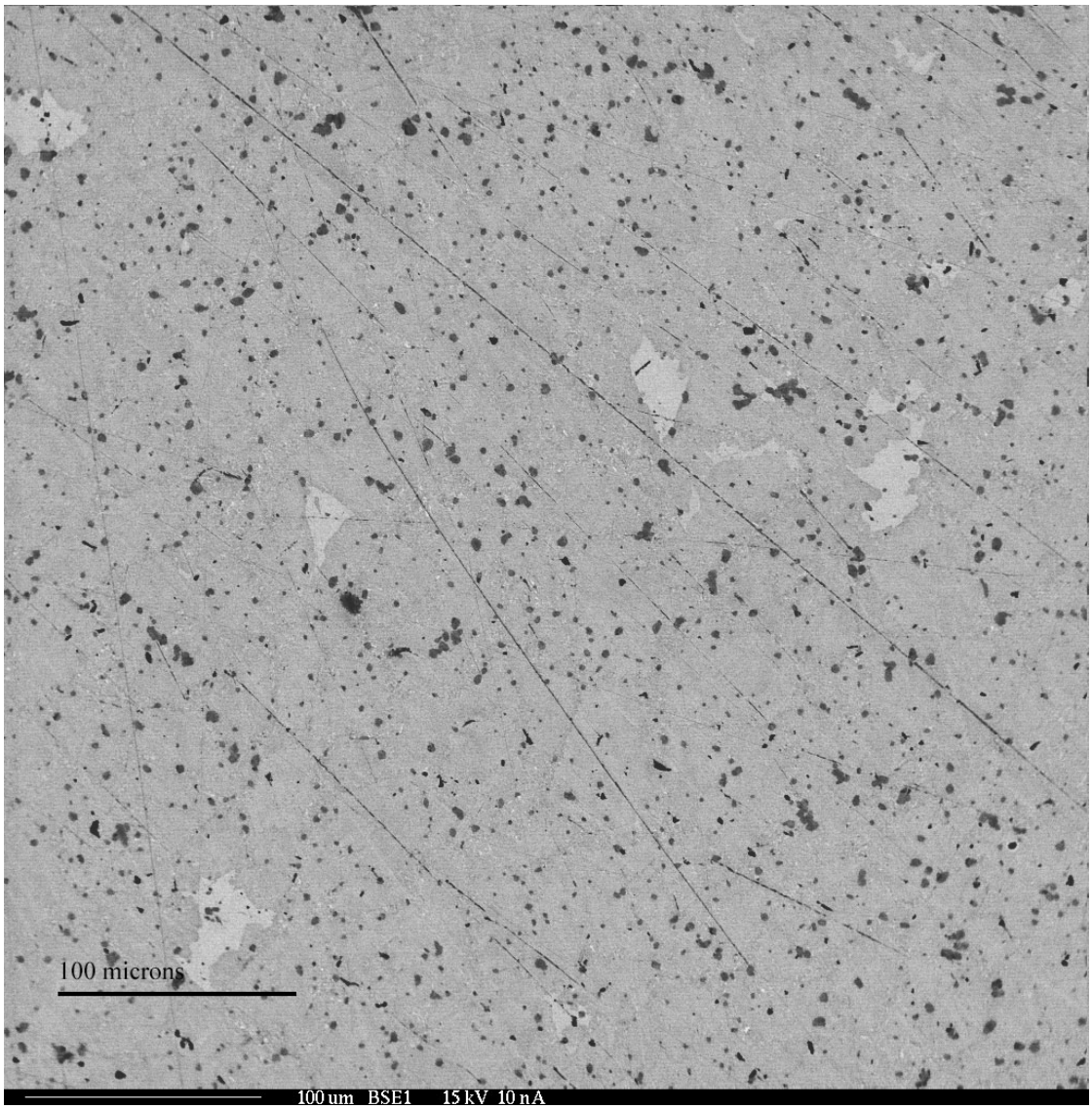

Figures 4-3: U-10Mo sample 3222, 97% gamma decomposed.

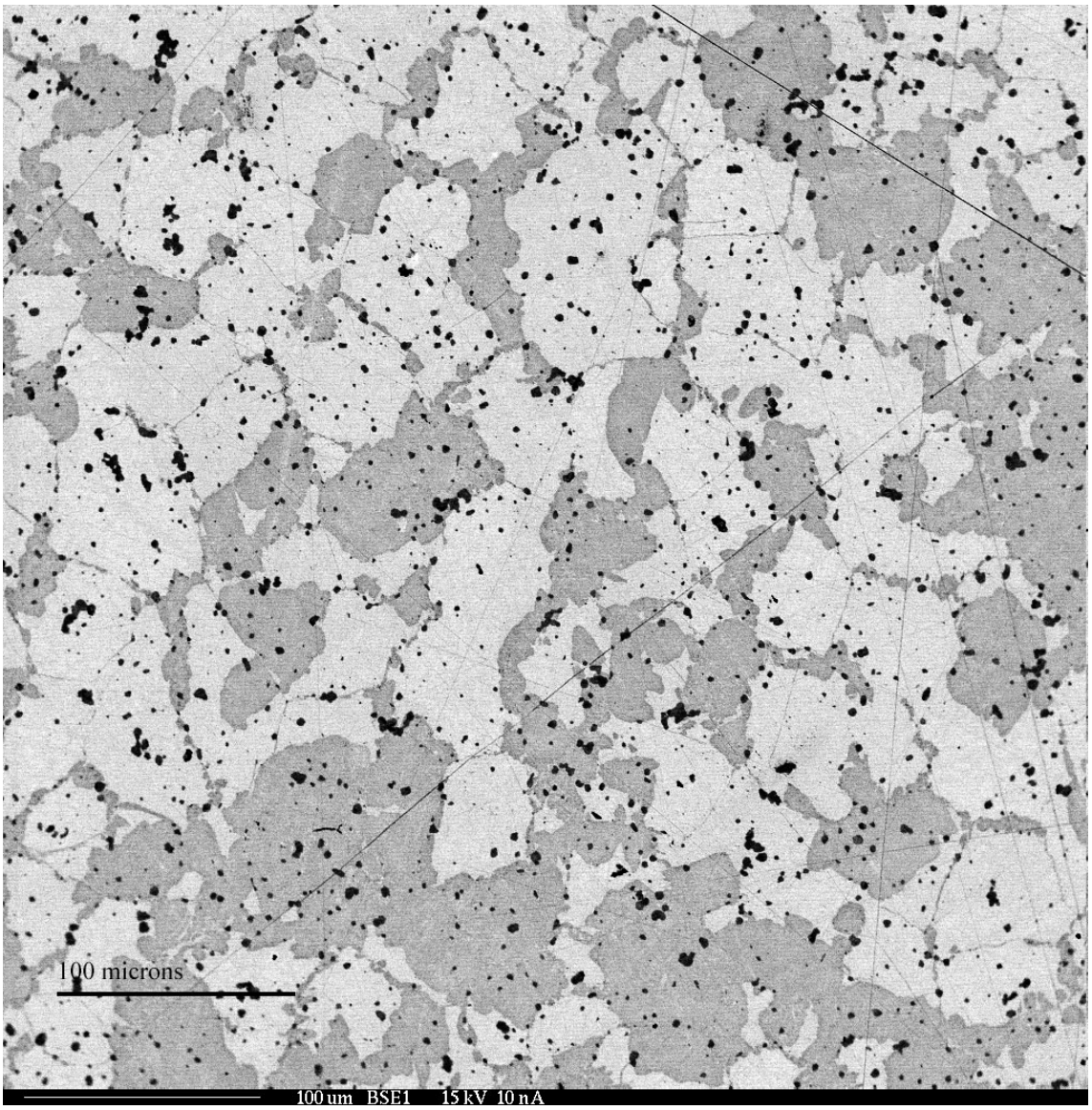

Figure 4-4: U-10Mo sample 3223, 47% gamma decomposed.

The gamma quenched U-10Mo sample shows no variation over the area of the sample, with the only notable feature being the presence of uranium carbide. The 96 hour at 500°C heat treatment shows extensive phase decomposition, with notable pockets of gamma phase grains remaining. The gamma phase present also appears to be

in the process of being overtaken by lamella of the alpha + U_2Mo phases extending into the grains. Estimates from image analysis of the microscopy images was used to calculate the values for gamma phase decomposition shown in Table 4-3 below.

Table 4-3: Percentage gamma phase decomposition for U-10Mo.

Sample	Alloy	Percent gamma decomposition
3221	U-10Mo	0.0%
3222	U-10Mo	97%
3223	U-10Mo	50.0%

4.2.3 U-10Mo Thermal Diffusivity Results

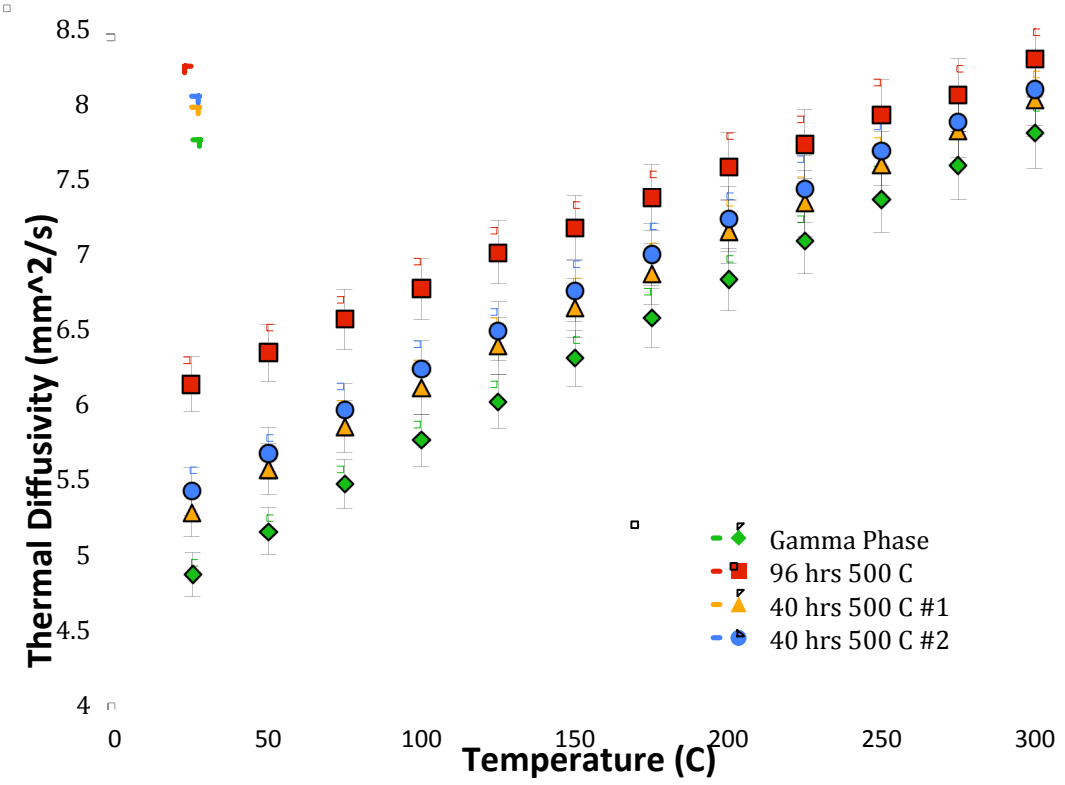

Figure 4-5: U-10Mo thermal diffusivity.

The thermal diffusivity measurements of the U-10Mo samples (Fig. 4-5) showed a consistent increase in thermal diffusivity with respect to decomposition time at 500°C.

4.2.4 U-10Mo Specific Heat Capacity Results

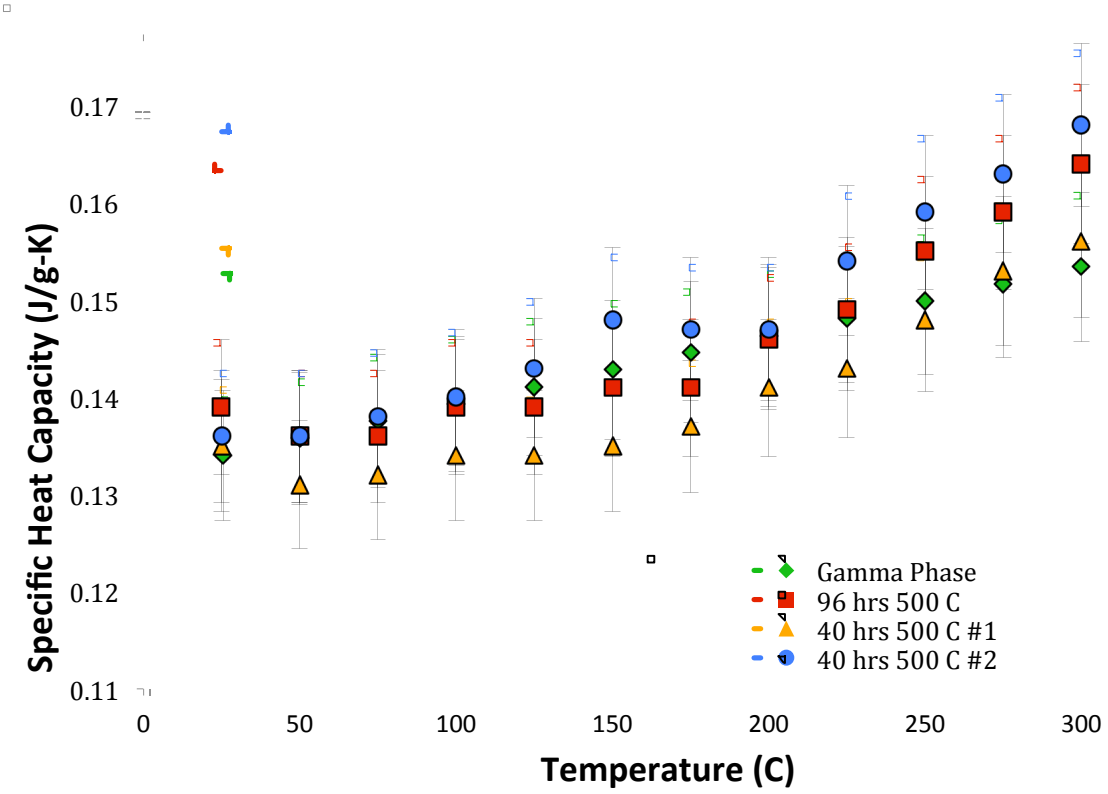

Figure 4-6: U-10Mo specific heat capacity.

The specific heat capacity approximations (Fig. 4-6) showed a relatively small variance between the gamma stabilized and heat treated samples. All values fall within the error range of one another.

4.2.5 U-10Mo Thermal Conductivity Results

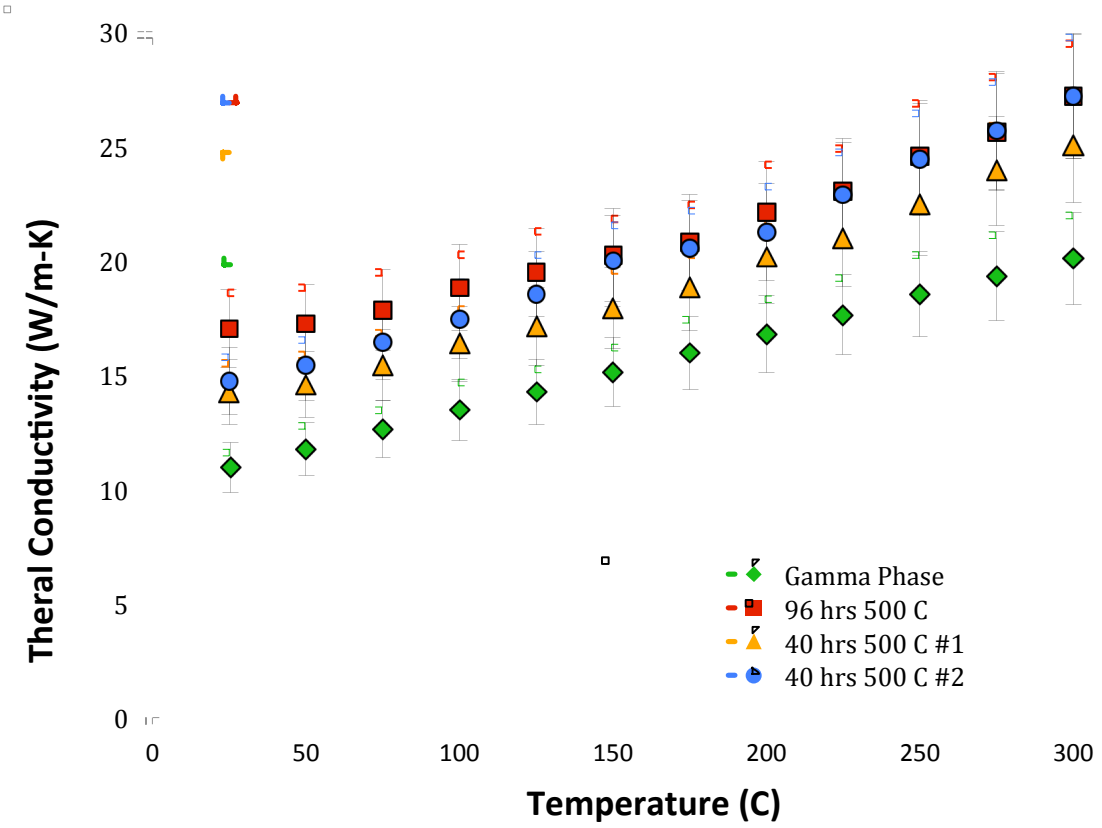

Figure 4-7: U-10Mo thermal conductivity.

The thermal conductivity measurements of the U-10Mo samples (Fig. 4-7) show a steady increase in thermal conductivity with respect to decomposition time at 500°C.

4.3 U-7Mo Results

4.3.1 XRD Results

In sample 321.1, which was U-7Mo gamma stabilized, the sole presence of the gamma phase was confirmed. In sample 321.2, which was heat treated at 500°C for 96

hours. The presence of the alpha phase and U_2Mo was confirmed. Sample 3213 and 3214, heat treated for 5 and 14 hours at 500°C, respectively, showed the presence of U2Mo and alpha phase U-Mo. These results are tabulated below in Table 4-4.

Table 4-4: XRD results for U-7Mo.

U-7Mo	**Time @ 500 C**	**Phases Present**
Heat Treat 1	Quench	Gamma
Heat Treat 2	96 hours	gamma, alpha, U2Mo
Heat Treat 3	5 hours	gamma, alpha, U2Mo
Heat Treat 4	14 hours	gamma, alpha, U2Mo

4.3.2 Microscopy Results

The images taken at 200X magnification are presented below. The remainder of the images may be found in Appendix A.

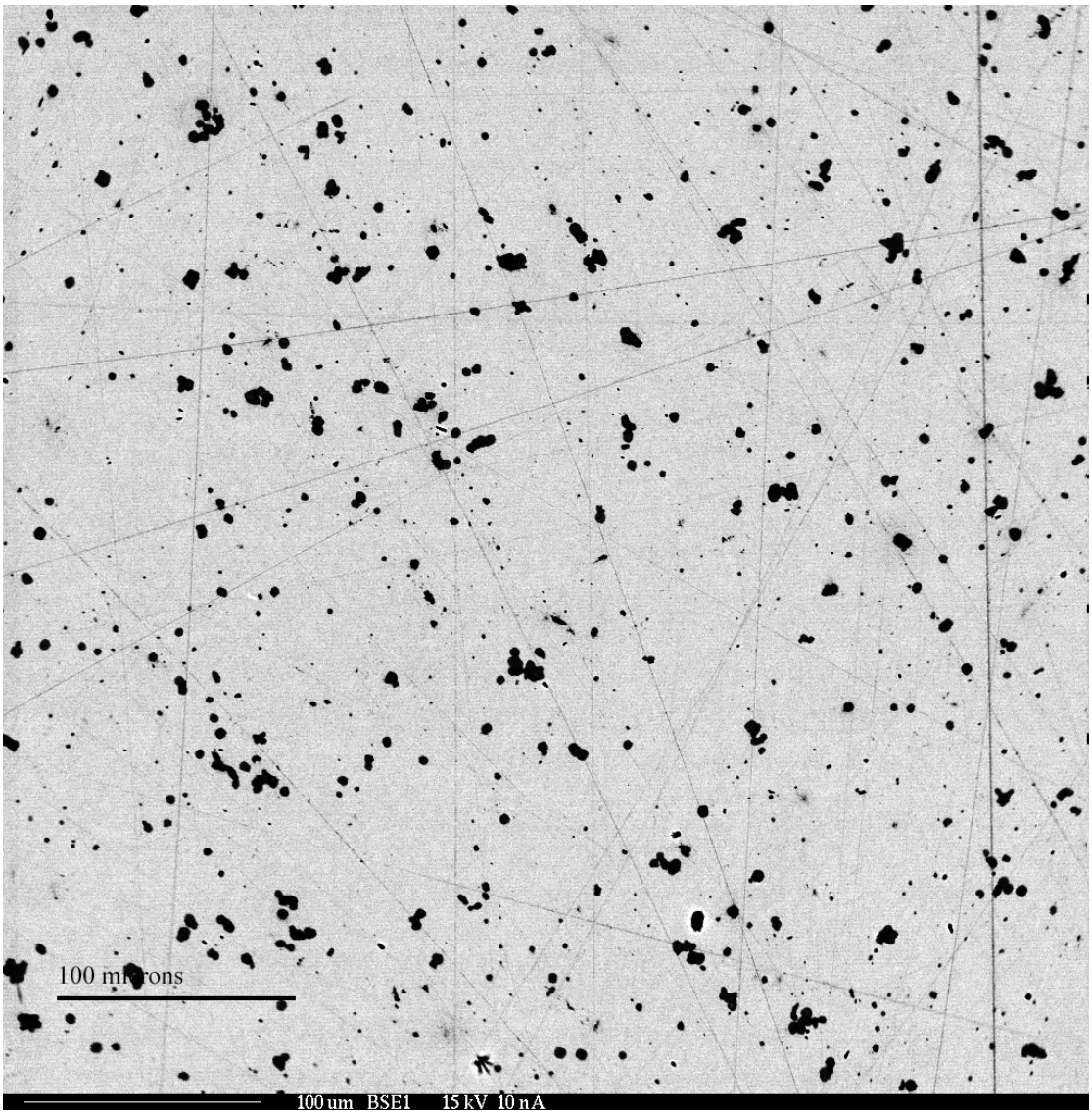

Figure 4-8: U-7Mo sample 3211 gamma phase.

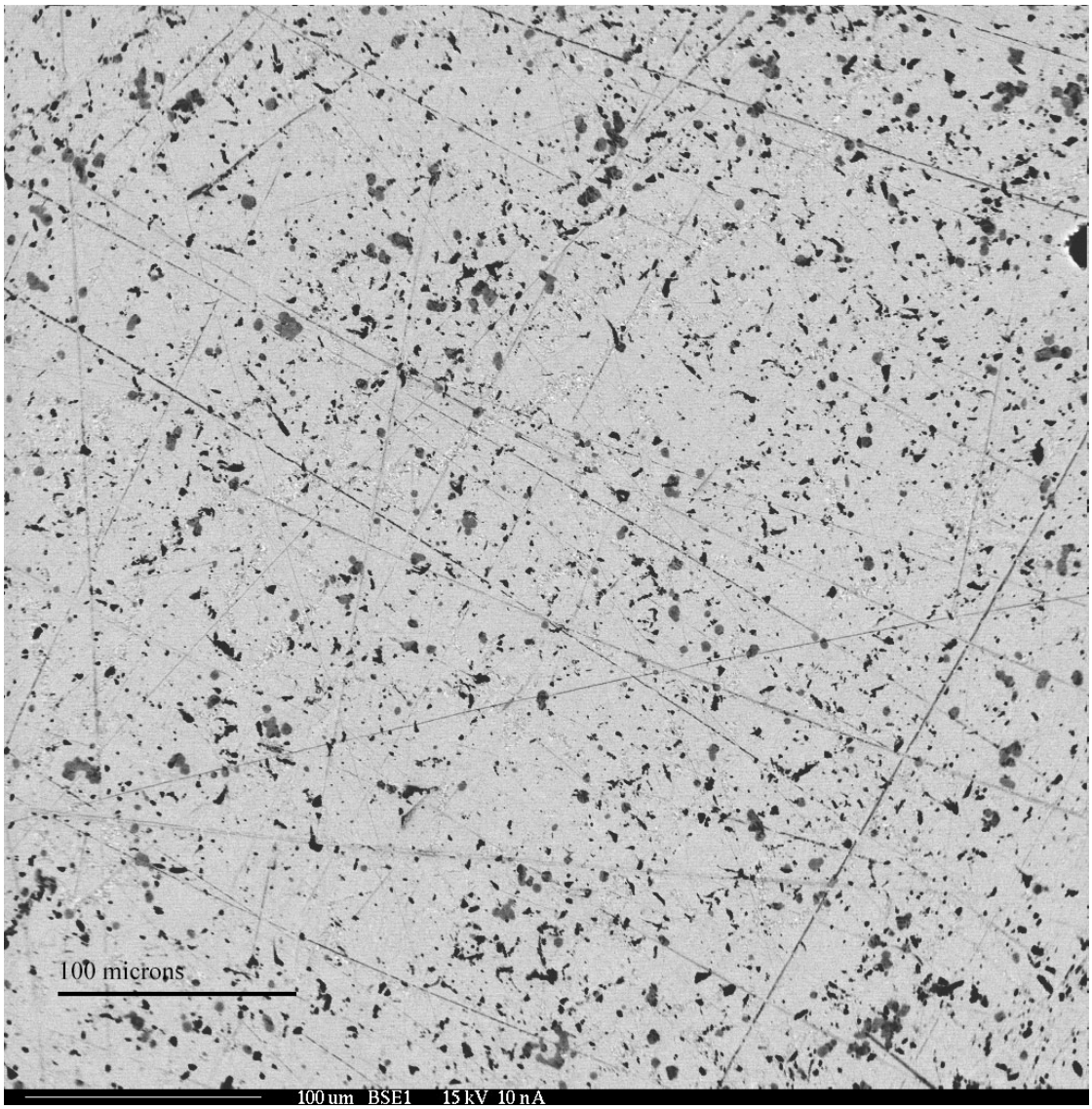

Figure 4-9: U-7Mo sample 3212 gamma decomposed.

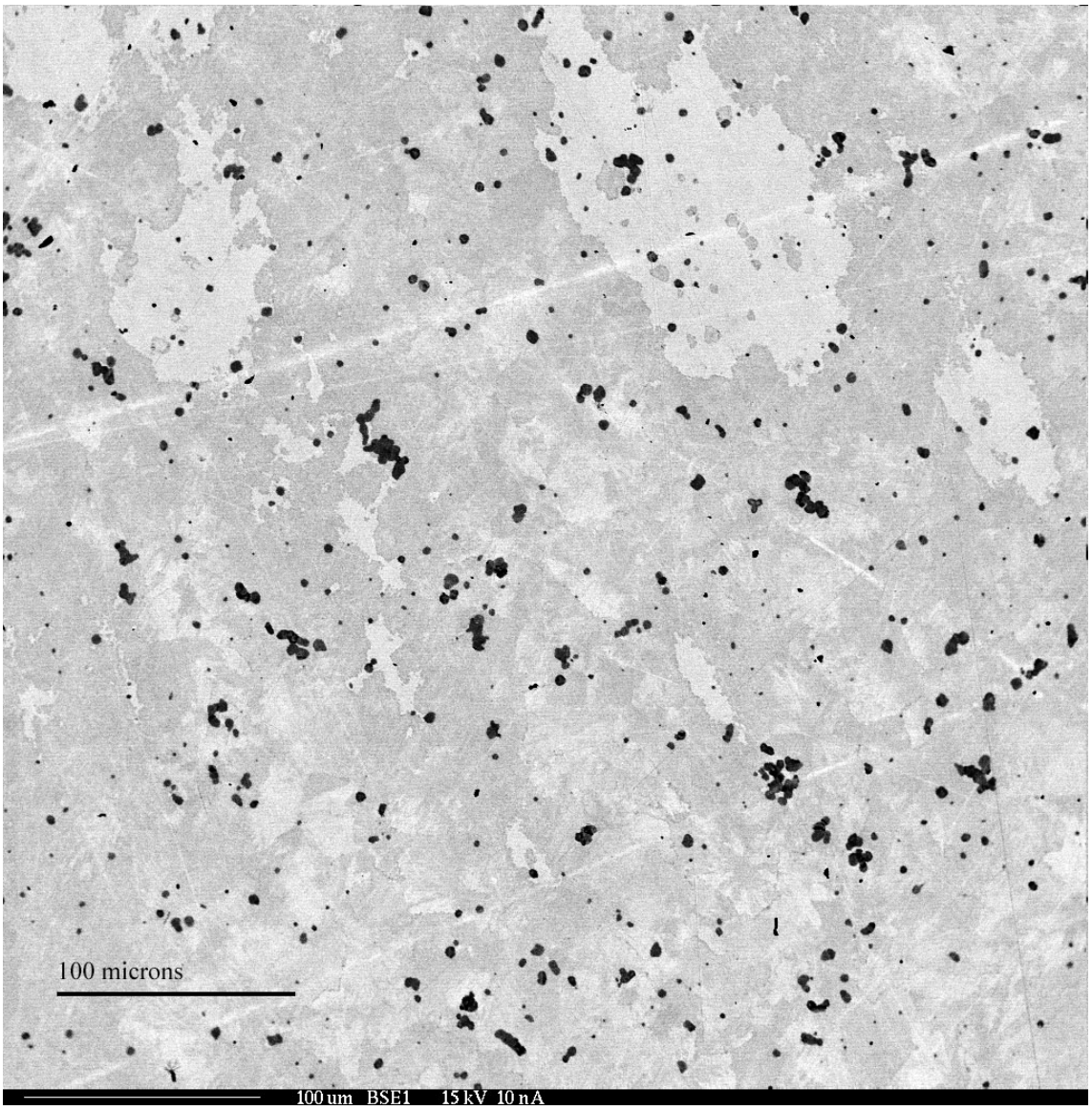

Figure 4-10: U-7Mo 3214, 68% gamma decomposed.

The U-7Mo gamma quenched microscopy sample showed no indication of gamma decomposition (Fig. 4-8), an observation backed up by the XRD data. The 96 hour at 500 C heat treatment appears to be completely decomposed into alpha + U_2Mo, as expected (Fig. 4-9). At higher magnification the texture of the microstructure for this

heat treatment is quite interesting. Some grains have a fine lamellar structure, while for others, a more coarse lamellar pattern is observed. This may be related to the grain orientation, size, and the texture of the grain boundary. The 14 hour at 500°C heat treatment resulted in approximately a 68% decomposition of the gamma phase (Fig. 4-10), with remaining grains of gamma phase interspersed throughout the matrix. As with the U-10Mo sample, the remaining gamma phase structure appeared to be in the process of decomposition into alpha + U_2Mo through grain boundary nucleation and subsequent growth of lamella into the grain. The resulting decompositions are displayed in Table 4-5 below.

Table 4-5: Percentage gamma decomposition for U-7Mo.

Sample	**Alloy**	**Percent gamma decomposition**
3211	U-7Mo	0.0%
3212	U-7Mo	100%
3213	U-7Mo	Not measured
3214	U-7Mo	68.5%

4.3.3 U-7Mo Thermal Diffusivity

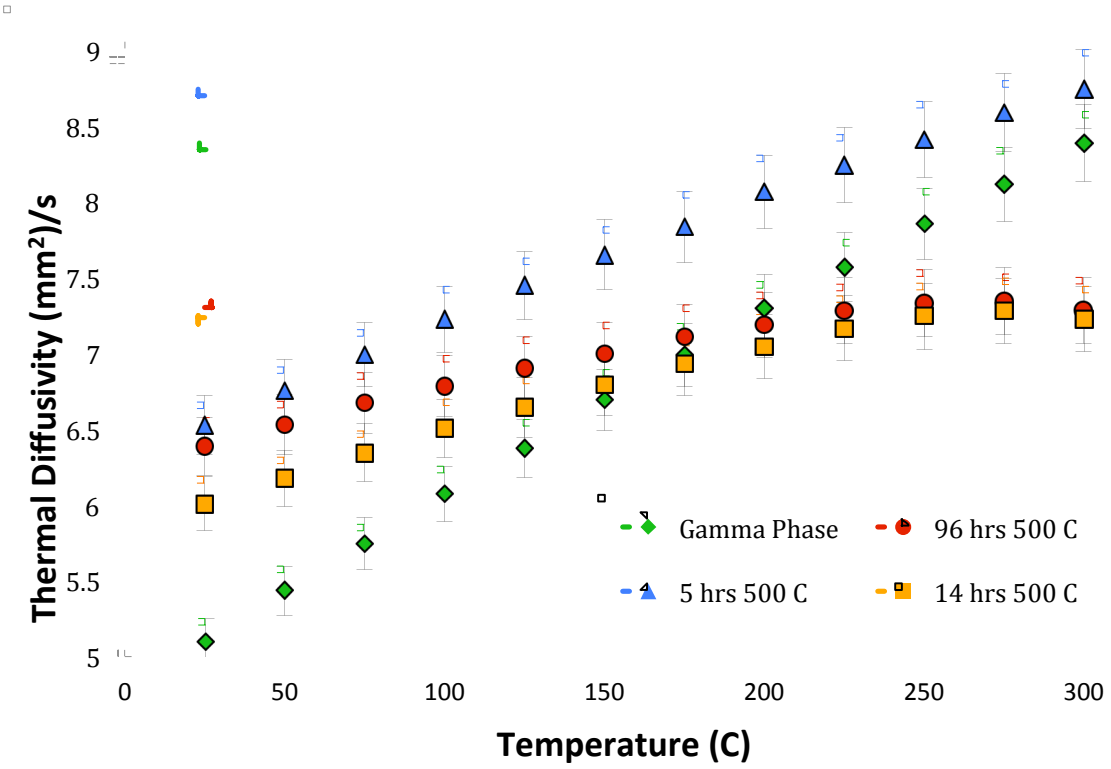

Figure 4-11: U-7Mo thermal diffusivity.

The thermal diffusivity measurements of U-7Mo (Fig. 4-11) show an initial increase in thermal diffusivity for the 5 hour decomposed samples, and then a subsequent flattening of the thermal diffusivity profile with the further heat treated samples.

4.3.4 U-7Mo Specific Heat Capacity

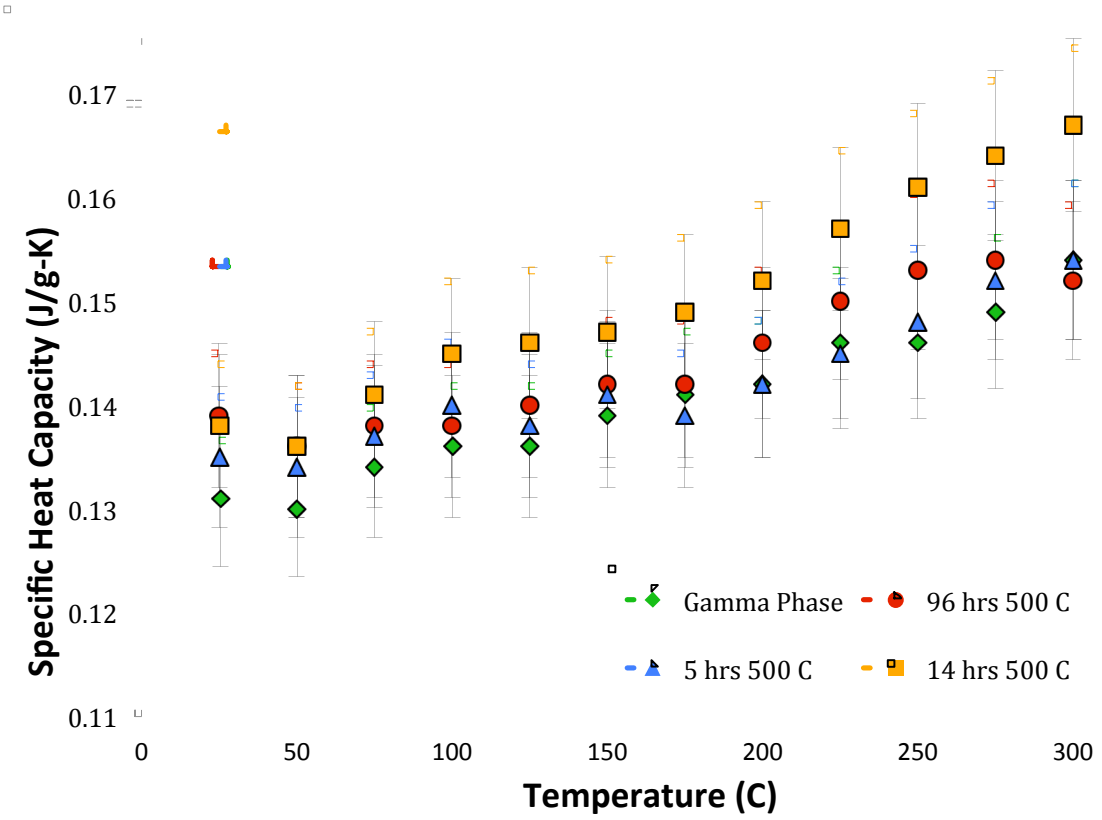

Figure 4-12: U-7Mo specific heat capacity.

The specific heat capacity approximations for the U-7Mo samples (Fig. 4-12) show a close grouping of the measurements to within the error bars of one another, with the exception of the 14 hour at 500°C sample. The 14 hour decomposed sample demonstrates an increase in specific heat capacity.

4.3.5 U-7Mo thermal conductivity

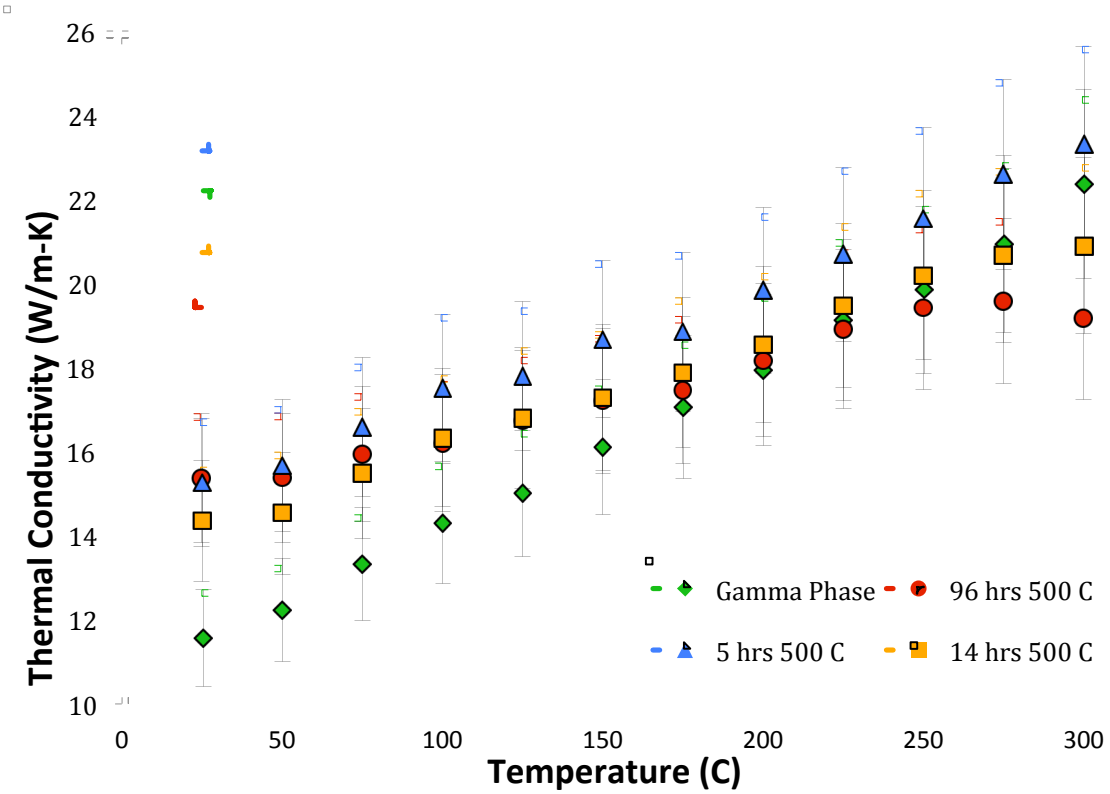

Figure 4-13: U-7Mo Thermal Conductivity.

The thermal conductivity of the U-7Mo samples (Fig. 4-13) shows an initial increase in thermal conductivity with respect to time at temperature, followed by a flattening of the thermal conductivity curve as the time at temperature increases.

4.4 U-13Mo Results

4.4.1 U-13Mo XRD Results

The X-ray diffraction results for the U-13Mo samples are shown in Table 4-6.

Table 4-6: XRD results for U-13Mo.

U-7Mo	**Time @ 500 C**	**Phases Present**
Heat Treat 1	Quench	Gamma, U2Mo
Heat Treat 2	166 hours	gamma, alpha, U2Mo

4.4.2 U-13Mo Microscopy Results

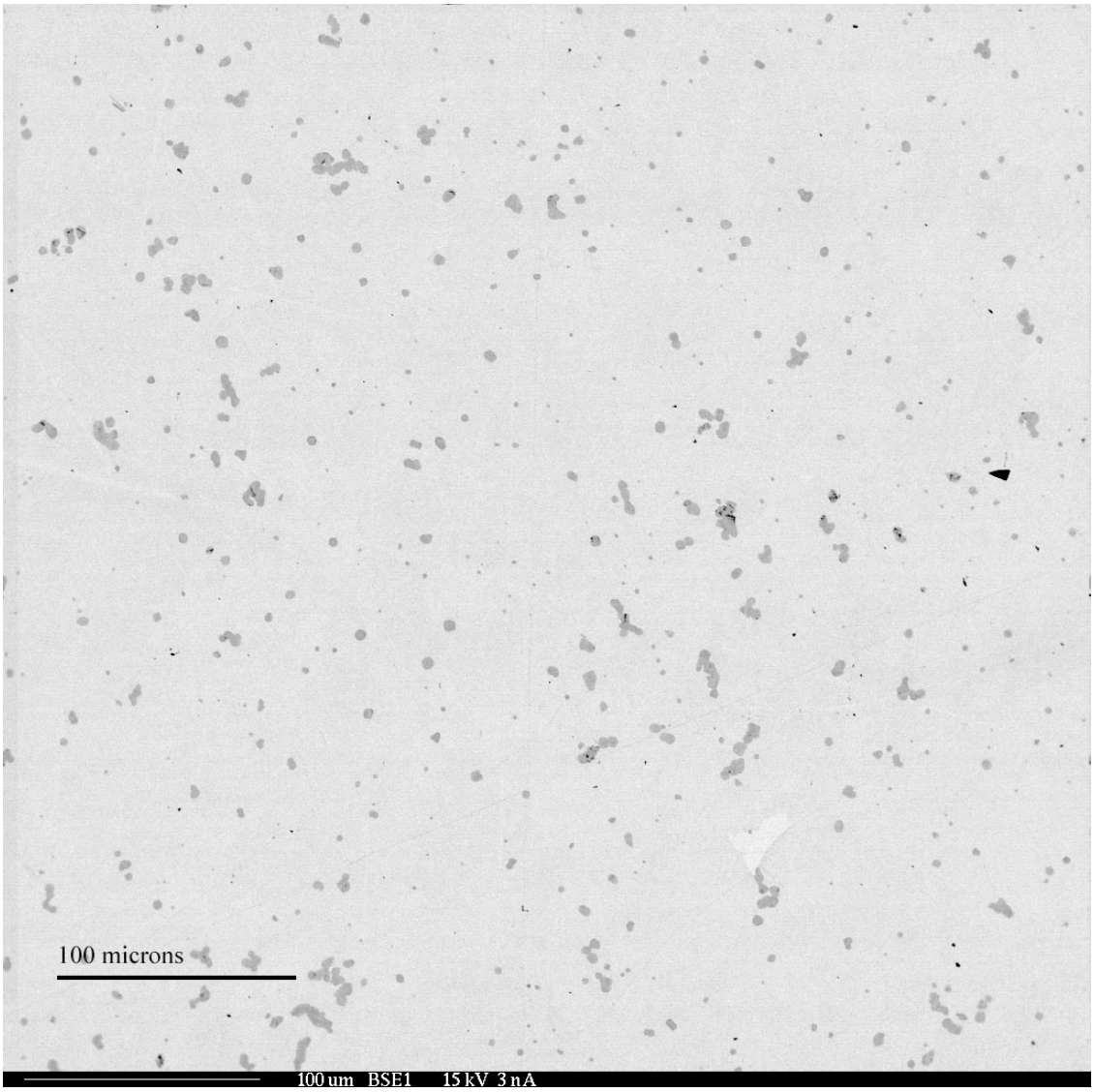

Figure 4-14: U-13Mo sample 3231 quenched.

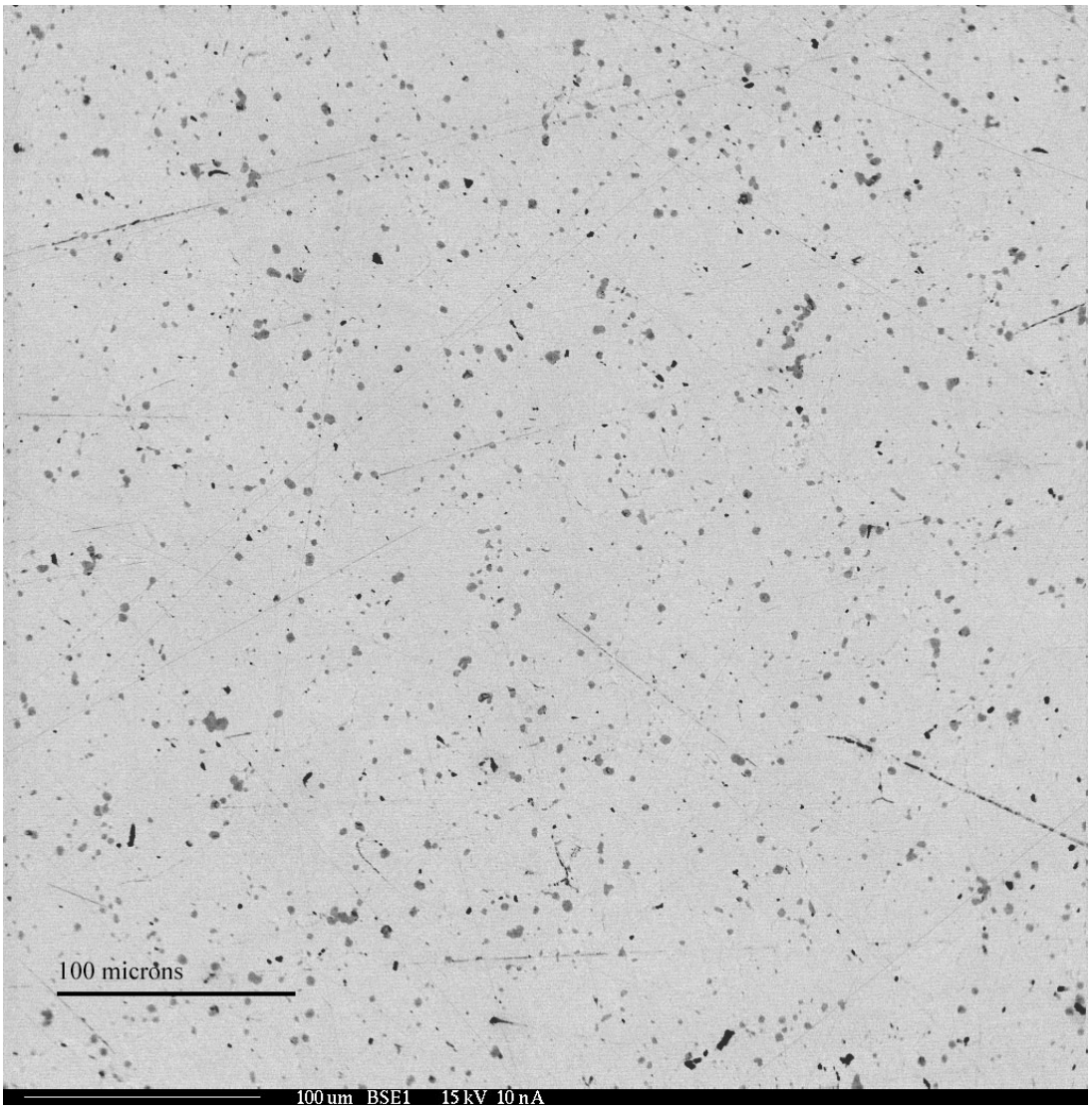

Figure 4-15: U-13Mo sample 3233, 1% gamma decomposed.

There are no notable features for the quenched U-13Mo sample (Fig. 4-14), as expected for the gamma phase. The 166 hour at 500 C heat treatment results in a grain boundary effect that may only be seen under high magnification (Fig. 4-15). It appears that nucleation of the alpha + U_2Mo phases is occurring at the grain boundary, but no

growth into the grains has begun. The gamma phase decomposition levels are detailed in Table 4-7.

Table 4-7: U-13Mo percentage phase decomposition.

Sample	Alloy	Percent gamma decomposition
3231	U-13Mo	0.0%
3232	U-13Mo	0%
3233	U-13Mo	1%
3234	U-13Mo	1%

4.4.3 U-13Mo Thermal Diffusivity Results

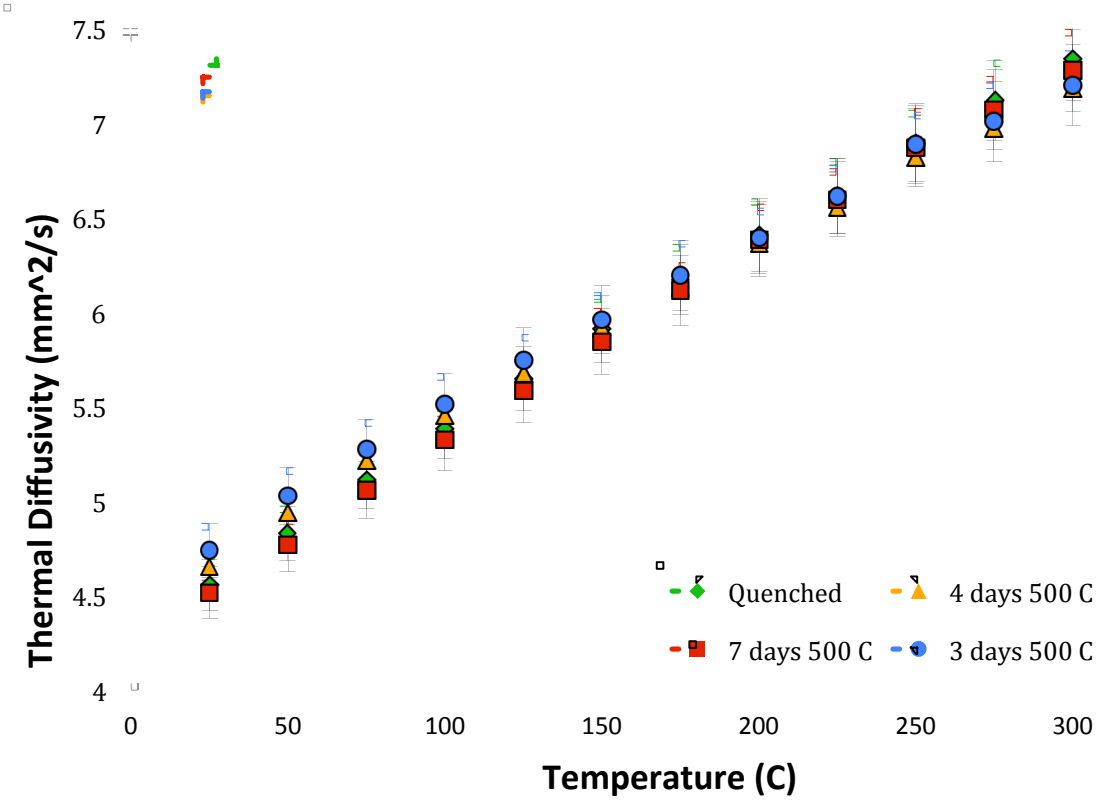

Figure 4-16: U-13Mo Thermal Diffusivity Data.

The thermal diffusivity measurements of the U-13Mo samples (Fig. 4-16) show a tight grouping of values within the error values of one another.

4.4.4 U-13Mo Specific Heat Capacity Results

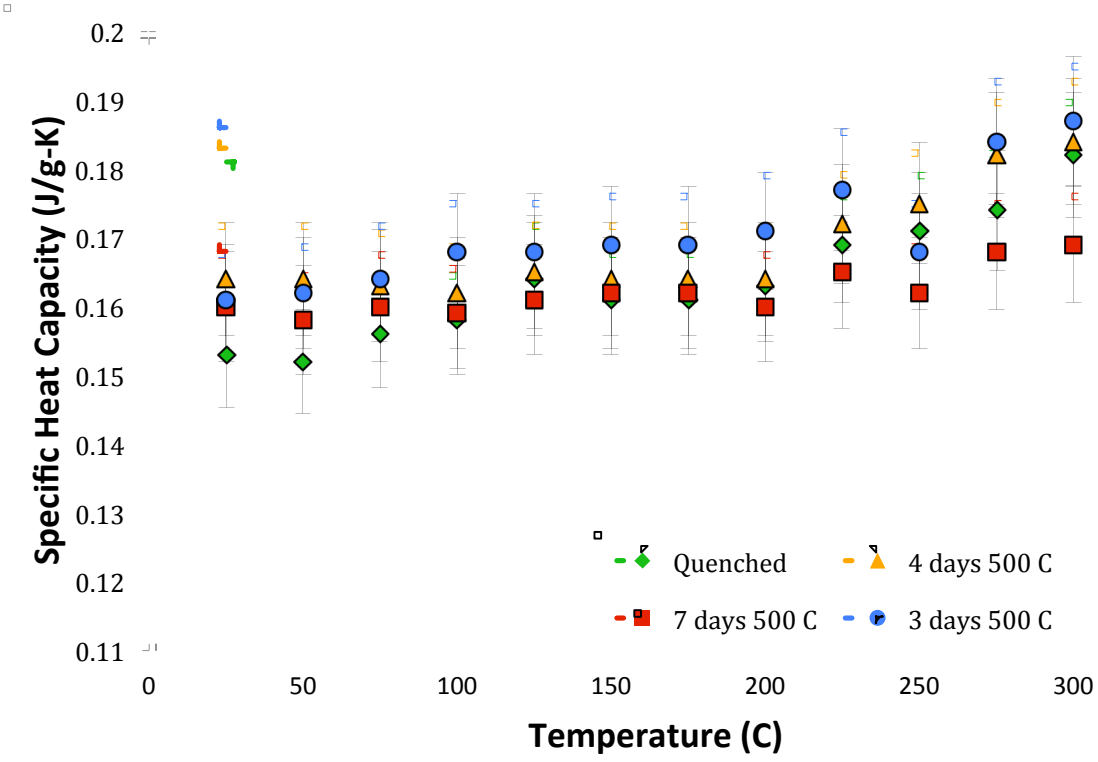

Figure 4-17: U-13Mo Specific Heat Capacity.

The specific heat capacity approximations for the U-13Mo samples (Fig. 4-17) show a tight grouping in which the values fall within the error range of one another.

4.4.5 Thermal Conductivity Results

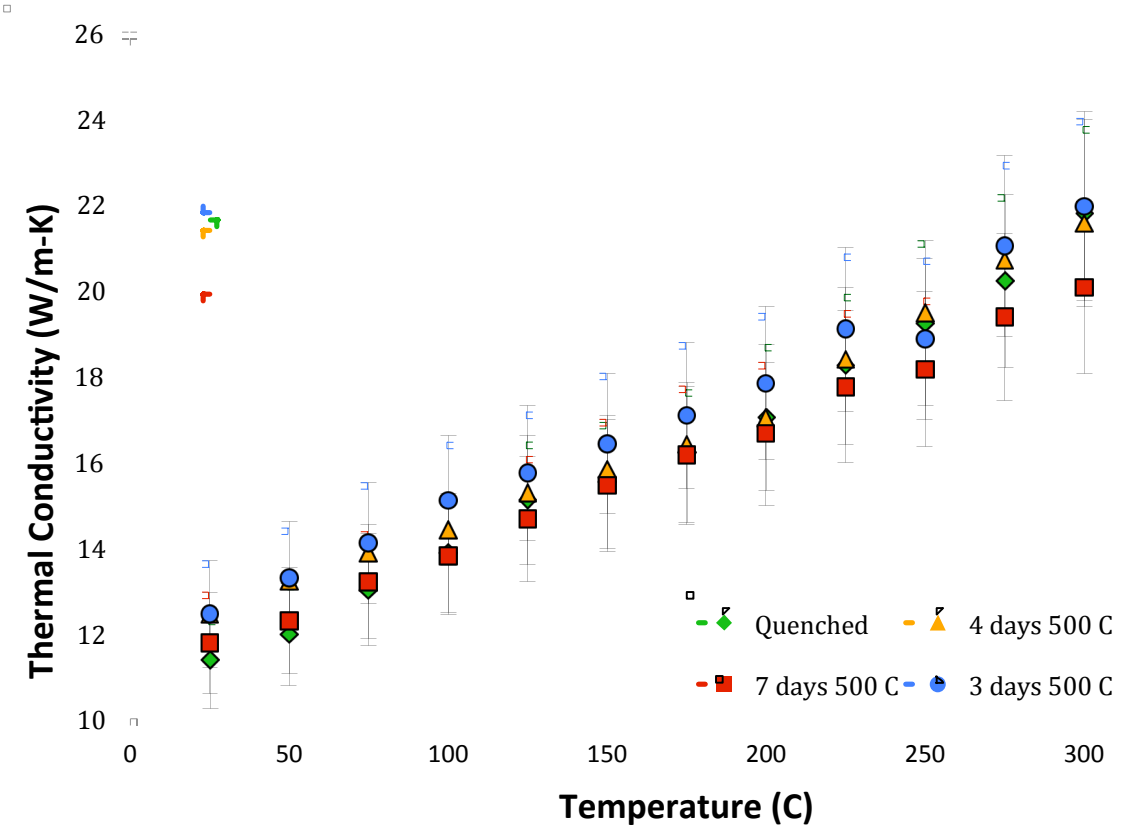

Figure 4-18: U-13Mo Thermal Conductivity.

The thermal conductivity measurements of the U-13Mo (Fig. 4-18) samples also show a tight grouping and fall within the error measurements of one another.

5. DISCUSSION

5.1 Microstructure

The grain structure from sample to sample showed some variance, although small. It is believed that the casting method and comparable cooling times between samples contributed to this grain structure. For example, a sample cast and cooled under forced convection would likely have smaller grains that a sample cooled in the furnace, since it would cool slower when held in the furnace.

Backscatter electron (BSE) imaging with the microprobe showed the phase regions very well on most of the samples, and analysis of the images allowed for quantification of the amount of gamma phase remaining in each sample. The EPMA was, however, unable to resolve the fine differences between the alpha and U_2Mo phases that existed in some of the lamellar structures observed.

The samples for XRD were not ground into powder, as is usually done for this XRD analysis, and thus any ordering of the phases in the samples would cause error in the results. It has been noted [12] that the gamma phase grains align themselves orthogonally to the direction of cooling. In the samples the cooling occurred radially. This would indicate that the round sample laid flat in the X-ray diffractometer should appear isotropic for the gamma phase. Unfortunately this still is unlikely to give an XRD spectrum with which a comparison of the quantity of each phase present may be calculated. The XRD spectra were still extremely useful in verifying the existence of the phases present in the material.

In the U-13Mo samples, it appears that there may have been some U_2Mo present in the gamma stabilized initial form. This was indicated in the XRD spectrum of one sample of the gamma quenched material, and further data was not collected to confirm the presence of U_2Mo. Variations in the matrix of the material which would indicate a second phase in the gamma stabilized material were not observed in the EPMA images. The duration of the homogenization heat treatment was on par with investigations conducted in the past for alloys of lesser molybdenum assay, and the near 14 wt% molybdenum in this sample may have needed additional time during the homogenization step.

The observed level of gamma decomposition appeared to agree with the predictions made in section 3.1.4 of the phase change with respect to time at temperature. The ability to quantitatively predict the phase decomposition of this alloy is instrumental for future processes that will use U-Mo. A desired state of the U-Mo to be produced is defined for a given production process. The process may be more readily optimized with the knowledge that the phase state of the U-Mo may be predicted. For example, if a U-Mo fuel is desired with all gamma phase material, and the process involves holding the material at and elevated temperature during a fabrication step, then an accurate prediction of the decomposition effects of the temperature allow for a process to be designed which will meet the requirement of not allowing the material to decompose from the gamma phase.

The additional data accumulation of both the decomposition at temperature with respect to time (TtT) and the thermophysical properties of the mixed phases will allow

for future models that define or predict the decomposition of U-Mo and the effects the decomposition will have on the resulting material. This may prove useful in future reactor designs in which temperature transients or holds could occur while the fission rate is low. When this occurs, the phase composition of the fuel may be uncertain without data about the alloy decomposition rates This may lead to unintended consequences such as fuel swelling and fission gas release. With the proper knowledge, the reactor may be more fully utilized and do so safely.

For the most part grain size was uniform across the samples, with one exclusion. The U-10Mo heat treated at 500°C for 40 hours (sample 3223), showed very interesting features. Not only was the grain structure visible to a high power optical microscope, the cross-section had distinct regions. The innermost region was approximately 55% gamma decomposed, this was followed by a ring of approximately 30% gamma decomposition. The outermost portion, however, showed an interesting textured effect, possibly a result of the thermal cycling of the material. A composite image of sample 3223 is shown in Appendix A, Fig. A-9.

An additional interesting observation related to the alloy microstructure was related to the hardness of the material. Although there were too many variables (blade speed and sharpening, variances in alloys) to quantify the effect, the cutting time necessary to cut the samples appeared to increase with respect to level of phase decomposition. Discussions with TAMU and INL expertise indicated that previous experiences with the alloys would suggest that alpha phase precipitation in the metal matrix may have caused this effect.

5.2 Thermophysical Properties

The thermal diffusivity of the samples is presented in Figs. 4-5 through 4-18. The samples occasionally had delamination of the graphite coating, which can cause errors in the measured thermal diffusivity. Delamination occurs when residual volatiles remain behind on the sample and coating, and vaporize during the heating process to take thermal diffusivity measurements.

The U-10Mo samples showed a trend of increased thermal diffusivity with respect to time at temperature. This equated to an increase in thermal conductivity of the more phase decomposed samples, contrary to expectations of a decrease in thermal diffusivity and conductivity due to the larger number of interfaces within the microstructure. The U-10Mo also decomposed from the gamma to the alpha + U_2Mo phases at a slower rate than expected. This may have been due to the actual molybdenum assay on the order of 11%.

Little change was observed between the quenched and longest duration heat treatment for the U-13Mo alloy. This was expected following microprobe analysis indicating a higher molybdenum concentration (~14%). This higher concentration results in an estimated 200 day heat treatment at 500°C required to approach full gamma phase decomposition.

The U-7Mo had the most complete range of gamma phase decomposition out of the three alloys, and the gamma phase decomposed very rapidly compared to the other alloys. The thermal diffusivity and conductivity appear to flatten as higher levels of gamma phase decomposition occur. This may be related to the alloy beginning to reach

equilibrium conditions for its molybdenum content, or have something to do with the difference of U-7Mo from the eutectoid concentration (~10%). This could result in a different lamellar morphology and alter the thermal properties.

Very little change was observed between the quenched and longest duration heat treatment for the U-13Mo alloy. This was expected following microprobe analysis indicating a higher molybdenum concentration (~14%). This higher concentration results in an estimated 200 day heat treatment at 500°C required to approach full gamma phase decomposition.

The gamma phase thermal diffusivities at 25°C for the 7, 10 and 13 wt% alloys were 5.1, 4.8, and 4.5 mm^2/s respectively, and 8.4, 7.8, and 7.3 mm^2/s at 300°C. It is apparent that an increase in molybdenum content suppresses the thermal diffusivity for these samples.

When the U-7Mo and U-10Mo samples consisting of almost entirely alpha + U_2Mo are compared, the 25°C thermal diffusivity of U-7Mo increases from 5.1 to 6.4 mm^2/s but decreases from 8.4 to 7.3 mm^2/s at 300°C, while the U-10Mo increases from 4.8 to 6.2 mm^2/s at 25°C and increases from 7.8 to 8.3 mm^2/s at 300°C. The difference for the U-10Mo decreases with increasing temperature, but the U-7Mo sees an inversion of the difference between the gamma and the gamma decomposed samples.

Varying lamellar morphology, such as consistent one half micron thick lamella as opposed to random inconsistent lamella ranging from one to 3 microns thick, could have notable effects on the thermophysical properties of U-Mo alloys. The basis for this argument lies in the theory that thermal energy transport through dissimilar materials,

even slight dissimilarities, will be different than the thermal energy transport through a consistent material (assuming all other variables remain constant). This is analogous to energy transport through a layered material as opposed to one solid slab. Further understanding of these effects in uranium-molybdenum alloys would be insightful.

6. SUMMARY

The ability to homogenize and stabilize U-Mo in the gamma phase was demonstrated, as well as the controlled decomposition of the gamma phase into the alpha phase as well as U_2Mo. The lamellar structure of the decomposition of the gamma phase and introduction of the alpha phase beginning at the grain boundaries was observed, although the differentiation between the alpha and gamma prime phases was not made. The martensitic structure of the alpha plus gamma prime phase was very fine, and was beyond the capability of the EPMA to analyze individual fingers of the martensitic structure.

6.1 Microscopy

The images obtained through EPMA were very telling in that the progression of the gamma phase decomposition could be observed. The very fine (sub-micron) lamellar structure of the decomposition created some difficulty in estimating the progress of the phase change.

The samples each had approximately 0.9 wt% more molybdenum per sample than originally expected, and this is expected to slightly skew the data and correlations.

6.2 Thermophysical Properties

Thermal diffusivity of the samples was determined, and the decay of the samples generally resulted in an increase in thermal diffusivity. In the samples with longer duration decays, the thermal diffusivity appeared to flatten. This may be due to the growth of the alpha and U_2Mo phase into the matrix as the phase decomposition of the gamma phase completes. Howlett noted “The transformation taking place at lower

temperatures is complex in nature and appears to have an expansive and contractive component[15]". This is in reference to the nature of U-Mo to both expand and contract during the complex phase change between gamma and alpha plus U_2Mo.

Specific heat capacity changed with respect to molybdenum content, and reflects a conflict in literature[10, 11] in that specific heat trends up for some experimental methods when it should go down.

The density was expected to change slightly with decomposition of the gamma phase, but this was not observable within the inherent error of the measurement techniques used. Literature indicates that a dilatometer is necessary for this measurement, as accuracies to below a one percent change are necessary[11, 16, 17].

6.3 Recommended Future Work

While this experiment provided valuable data and showed trends which require further study, the procedures performed should be repeated for a larger temperature range, up to at least 800°C. This will allow for more accurate correlations and a data set which will line up with a variety of reactor and fabrication line conditions.

There also appears to be a relation between grain size and the nucleation and subsequent growth rate of the alpha + U_2Mo phases. More research could be done in this area. By controlling the initial cooling of the cast sample, perhaps through different mold thicknesses, the grain size should increase for increased cooling time. An experiment set could then be created to isolate the grain size effects as they related to phase decomposition.

REFERENCES

[1] M.K.M. Gerard L. Hofman, Allison Ray, Design of High Density Gamma-Phases Uranium Alloys for LEU Dispersion Fuel Applications, in Proceedings of the 1998 International Reduced Enrichment for Research and Test Reactors Conference, 18-20 October 1998, Sao Paulo, Brazil.

[2] J. Rest, Derivation of Analytical Expressions for the Network Dislocation Density, Change in Lattice Parameter, and for the Recrystallized Grain Size in Nuclear Fuels, Journal of Nuclear Materials, 349 (2006) 150-159.

[3] V. Kalashnikov, V. Titova, G. Sergeev, A. Samoilov, Uranium-Molybdenum Alloys in Reactor Construction, Atomic Energy, 5 (1959) 1315-1325.

[4] D. Burkes, R. Prabhakaran, J. Jue, F. Rice, Mechanical Properties of DU-x Mo Alloys with x= 7 to 12 Weight Percent, Metallurgical and Materials Transactions A, 40 (2009) 1069-1079.

[5] S. L. Fawcett, A Study of Core Fuel Systems for a Fast Breeder Power Reactor, in report BMI-APDA-636, Battelle Memorial Inst., Columbus, Ohio, 1957.

[6] Y. Goldstein, A. Bar-Or, Decomposition of Gamma Phase in Uranium Alloys Containing 8, 10.8, and 14.3 wt.-% Molybdenum, Journal of the Institute of Metals, (1967) 17-21.

[7] S.C. Parida, S. Dash, Z. Singh, R. Prasad, V. Venugopal, Thermodynamic Studies on Uranium-Molybdenum Alloys, Journal of Physics and Chemistry of Solids, 62 (2001) 585-597.

[8] D.E. Burkes, C.A. Papesch, A.P. Maddison, T. Hartmann, F.J. Rice, Thermo-physical Properties of DU-10†wt.% Mo Alloys, Journal of Nuclear Materials, 403 (2010) 160-166.

[9] K.H. Kim, D.B. Lee, C.K. Kim, G.E. Hofman, K.W. Paik, Characterization of U-2 wt% Mo and U-10 wt% Mo Alloy Powders Prepared by Centrifugal Atomization, Journal of Nuclear Materials, 245 (1997) 179-184.

[10] J.J. Rechtien, Nelson, R.D., Phase Transformations in Uranium, Plutonium, and Neptunium, Mettalurgical Transactions, 4 (1973) 2756 - 2766.

[11] H.L. Yakel, A Review of X-ray Diffraction Studies in Uranium Alloys, in Proceedings of the Physical Metallurgy of Uranium Alloys Conference Sponsored by the AEC, Army Material and Mechanical Research Center, 12-14 February, 1974, Vail, Colorado.

[12] E.K. Halteman, The Crystal Structure of U2Mo, Westinghouse Electric Corporation, Pittsburgh, Pennsylvania, 1956.

[13] J. Rest, Y.S. Kim, G.L. Hofman, M.K. Meyer, S.L. Hayes, U-Mo Fuels Handbook, Argonne National Laboratory and Idaho National Laboratory, 2006.

[14] A.E. Dwight, The Uranium-Molybdenum Equilibrium Diagram Below 900 C, Journal of Nuclear Materials, 2 (1960) 81-87.

[15] B.W. Howlett, A Study of the Shear Transformations from the Gamma-Phase in Uranium-Molybdenum Alloys Containing 6.0-12.5 at % Molybdenum, Journal of Nuclear Materials, 35 (1970) 278-292.

[16] B.W. Howlett, A.J. Eycott, I.K. Kang, D.R.F. West, The Kinetics of the Isothermal Decomposition of a Gamma-Phase Uranium - 6 Atomic % Molybdenum Alloy, Journal of Nuclear Materials, 9 (1963) 143-154.

[17] O.S. Ivanov, Y.S. Virgiliev, The Decomposition of the [Gamma]-Uranium Base Solid Solutions as Revealed by X-ray Investigations, Journal of Nuclear Materials, 6 (1962) 199-202.

[18] V.K. Orlov, V.M. Teplinskaya, N.T. Chebotarev, Decomposition of a Metastable Solid Solution in Uranium-Molybdenum Alloy, Atomic Energy, 88 (2000).

[19] A. Ray, G. Hofman, Design of Gamma-Phase High Density Uranium Alloys for LEU Dispersion Fuel Applications, Argonne National Laboratory, Chicago, 1998.

[20] C. Peterson, W. Steele, S. DiGiallonardo, Isothermal Transformation Study of Some Uranium-Base Alloys, in Report UCRL-7824, California University, Livermore, Lawrence Radiation Lab, 1964.

[21] J.J. Burke, D.A. Colling, A.E. Gorum, J. Greenspan (Ed.), Physical Metallurgy of Uranium Alloys, in Proceedings from the Third Army Materials Technology Conference, Brook Hill, 1976.

[22] H. Lee, J.M. Park, C.K. Kim, Thermophysical Properties of U–Mo/Al Alloy Dispersion Fuel Meats, International Journal of Thermophysics, 28 (2007).

[23] E.F.U.d.C. Fabio Branco Vaz de Oliviera, Humberto Gracher Riella, Fabrication Results of Gamma Uranium-Molybdenum Alloys Fuels, in Proceedings from the 2009 International Nuclear Atlantic Conference (INAC 2009), Rio de Janiero, Brazil, 2009.

[24] D. Keiser, S. Hayes, M. Meyer, C. Clark, High-density, Low-Enriched Uranium Fuel for Nuclear Research Reactors, Journal of the Minerals, Metals and Materials Society, 55 (2003) 55-58.

[25] M.C. AK Jena, Phase Transformations in Materials, Prentice Hall, 1992.

[26] R.A. Vandermeer, Recent Observations of Phase Transformations in a U-Nb-Zr Alloy*, Report 740205, Oak Ridge National Laboratory, Oak Ridge, Tennesee, 1973.

[27] Netzsch Group (Ed.), LFA 447 - Thermal Analysis, Handbook, NETZSCH-Geratebau GmbH, Selb/Germany, pp. 3.

[28] G.L. Hofman, A Short Note on High Density Dispersion Fuels, Internal Report, Argonne National Laboratory, Argonne, IL, 1996.

APPENDIX A

EPMA IMAGES

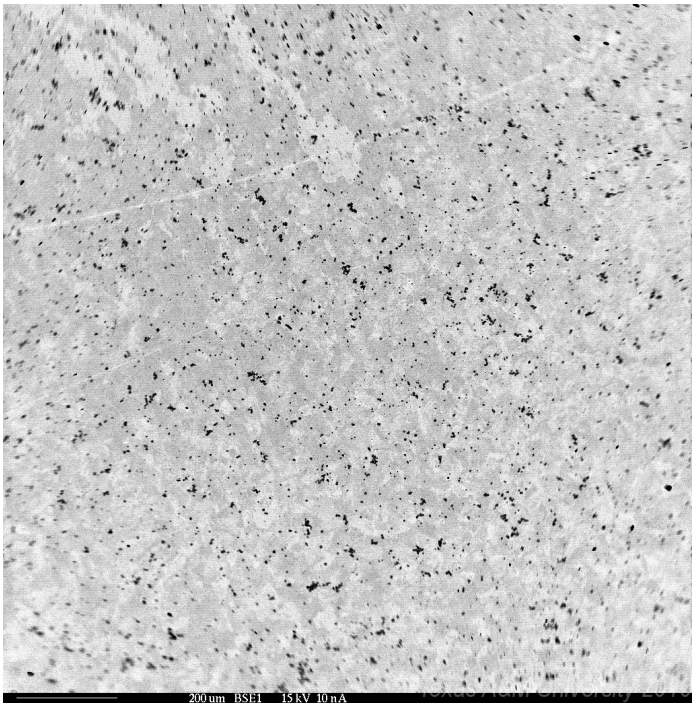

Figure A-1: Sample 3214 zone A at 67x magnification BSE

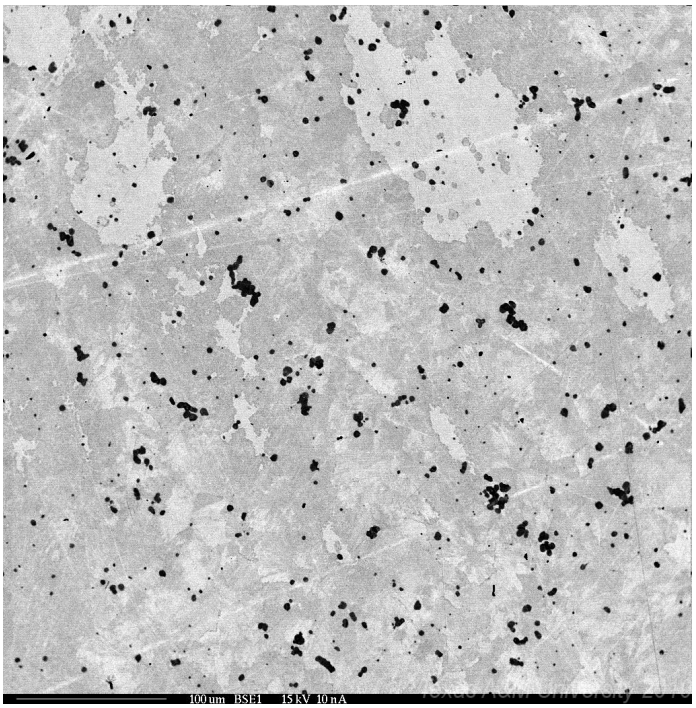

Figure A-2: Sample 3214 zone A at 200x magnification BSE

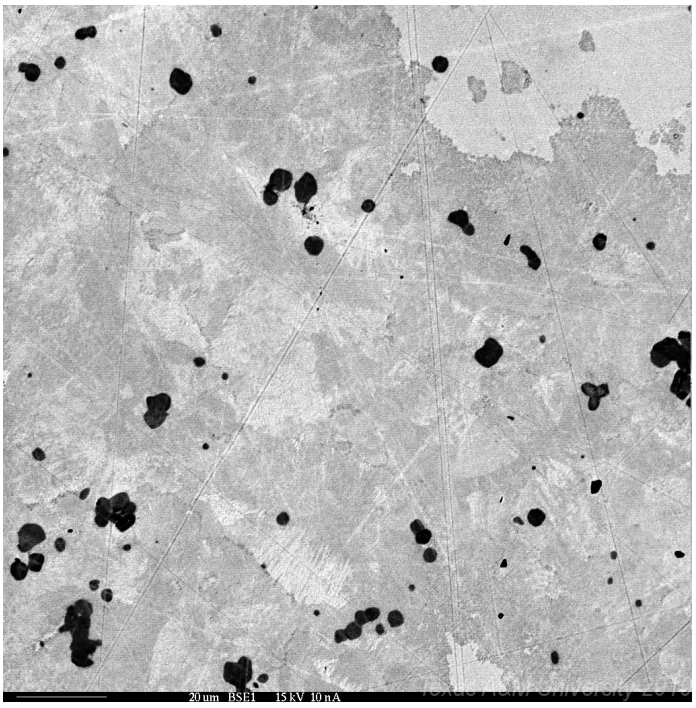

Figure A-3: Sample 3214 Zone A at 600X magnification BSE

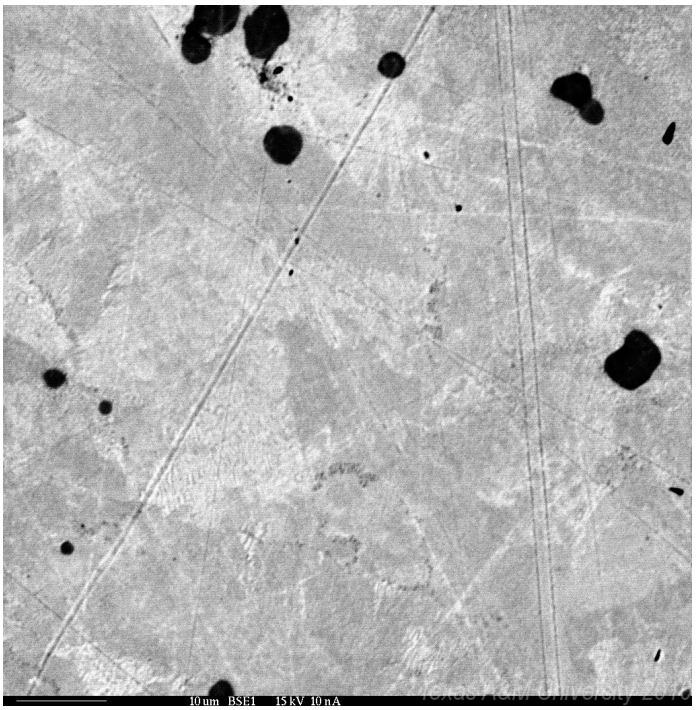

Figure A-4: Sample 3214 zone A at 1200X magnification

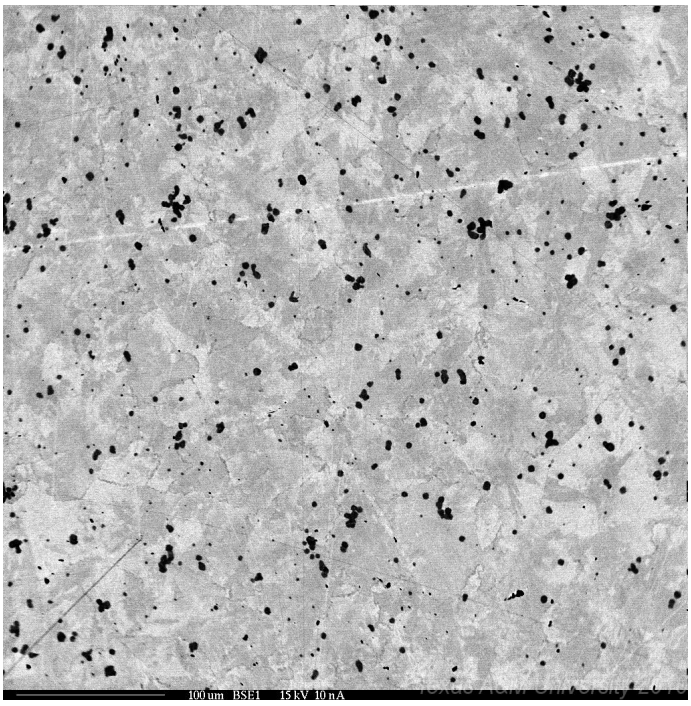

Figure A-5: Sample 3214 zone c at 200x magnification BSE

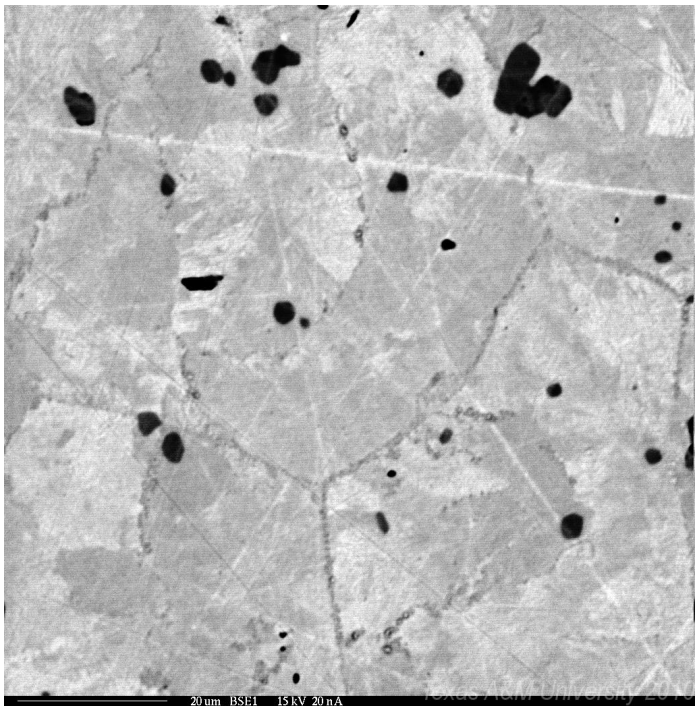

Figure A-6: 3214 zone D at 1000x magnification BSE

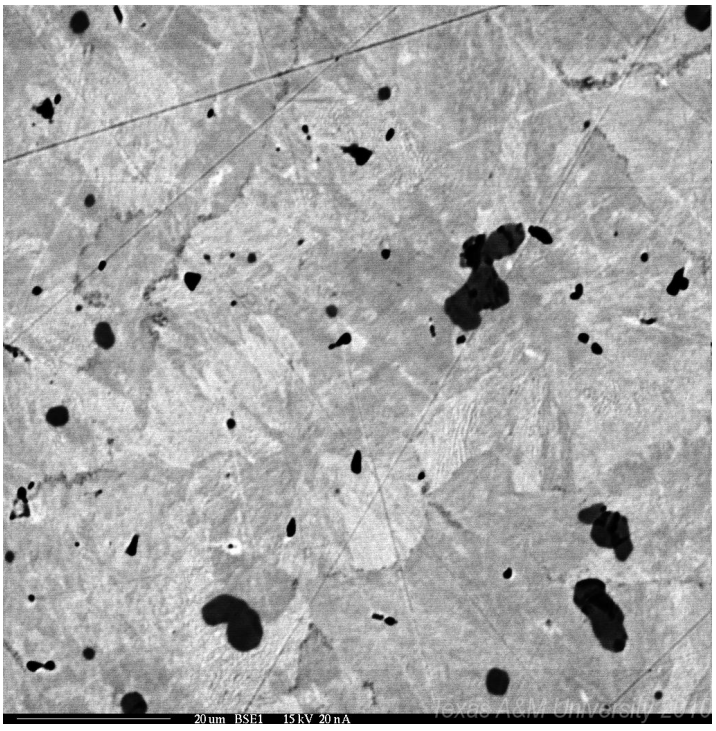

Figure A-7: 3214 zone B at 1000x magnification BSE

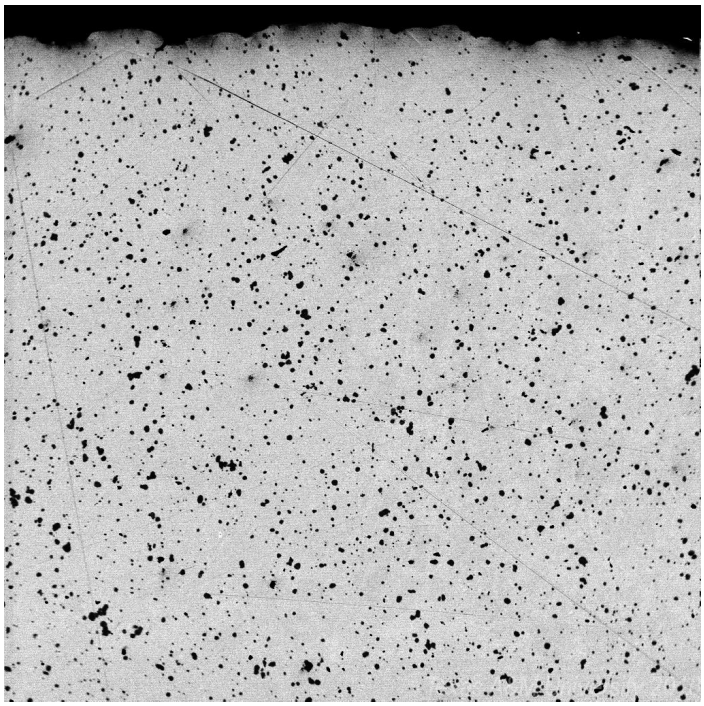

Figure A-8: Sample 3221 zone D at 200X magnification BSE

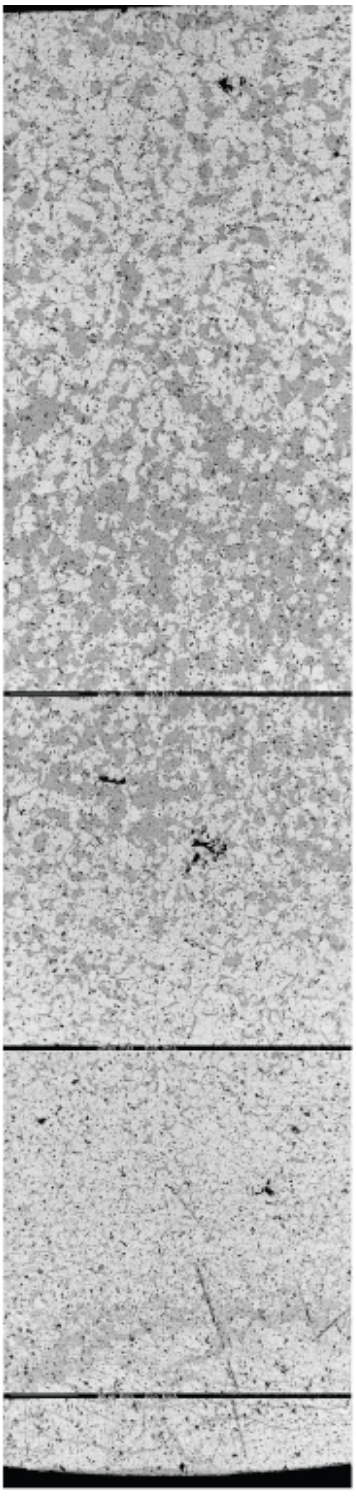

Figure A-9: Sample 3223 at 90X magnification BSE

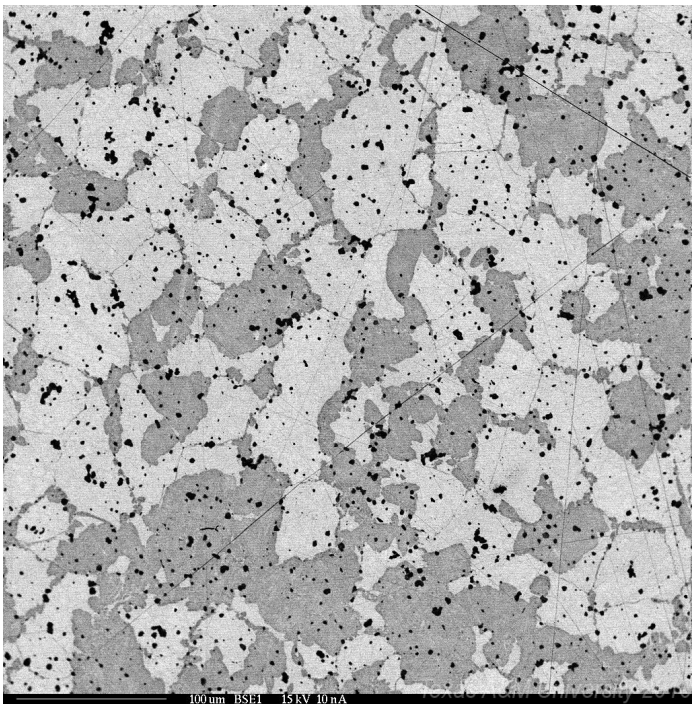

Figure A-10: Sample 3223 zone A at 200X magnification BSE

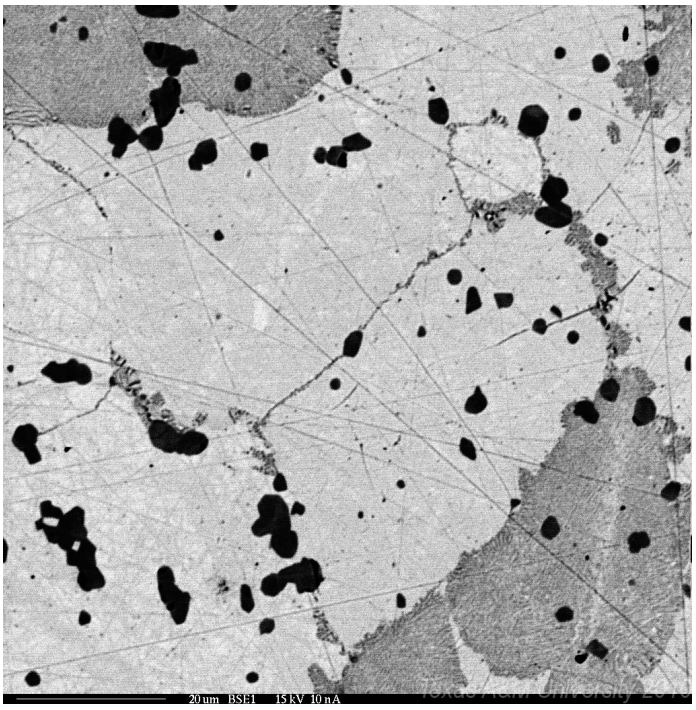

Figure A-11: Sample 3223 Zone A at 1000X magnification BSE

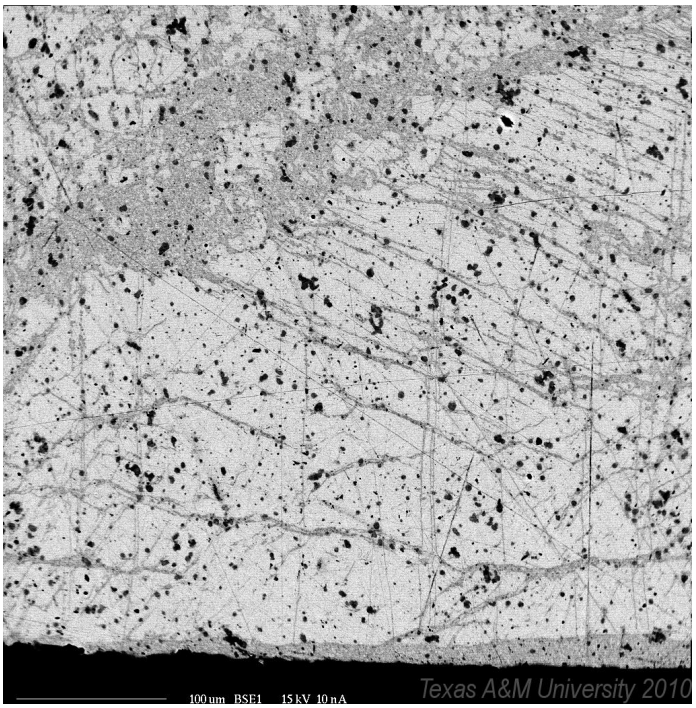

Figure A-12: Sample 3223 zone C at 200X magnification

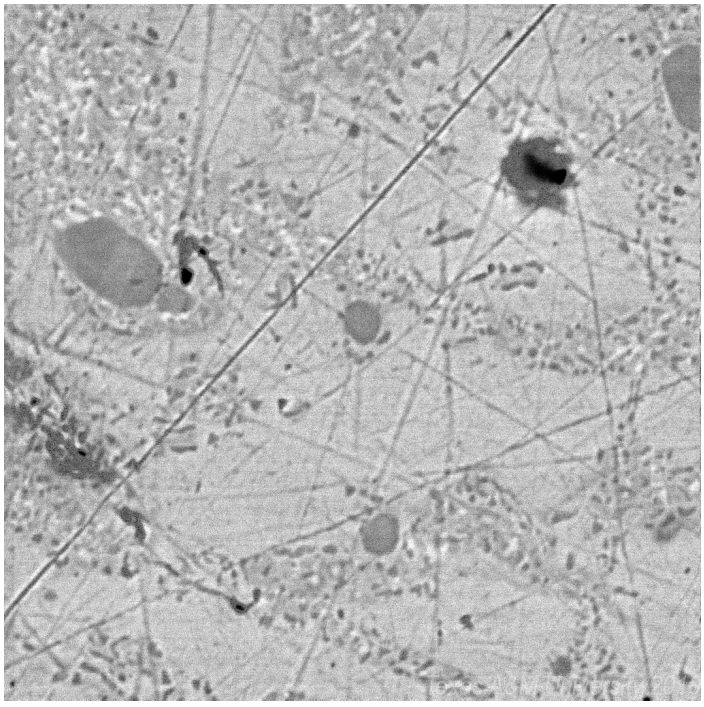

Figure A-13: Sample 3223 zone C at 4000X magnification BSE

APPENDIX B

WAVELENGTH DISPERSIVE SPECTROSCOPY MEASUREMENTS

Analysis	U (wt%)	Mo (wt%)	Total (wt%)	U (at%)	Mo (at%)
322.1 U-10Mo					
3221_pt1	89.83	11.00	100.83	76.71	23.30
3221_pt2	90.12	11.05	101.17	76.68	23.32
3221_pt3	89.61	10.90	100.51	76.81	23.19
3221_pt4	89.01	11.05	100.06	76.45	23.55
321.4 U-7Mo					
3214_pt1	91.53	7.91	99.44	82.34	17.66
3214_pt2	91.33	8.16	99.49	81.85	18.15
3214_pt2rpt	91.00	8.22	99.22	81.68	18.32
3214_pt1rpt	91.45	7.74	99.19	82.64	17.36
3214_pt1_50nA	92.44	7.84	100.28	82.61	17.39
3214_pt2_50nA	92.10	8.33	100.43	81.67	18.33
3214_pt3_50nA	92.29	8.12	100.41	82.08	17.92
3214_pt4_50nA	92.68	7.60	100.28	83.10	16.90
3214b_pt1_50nA	91.78	8.28	100.06	81.72	18.28
321.1 U-7Mo					
3211b_pt1_50nA	93.06	7.61	100.67	83.14	16.86
3211a_pt1_50nA	92.99	7.67	100.66	83.01	16.99
322.3 U-10Mo					
3223_b_pt1	89.63	11.05	100.68	76.57	23.43
3223_b_pt2	89.54	11.05	100.59	76.57	23.43
3223_b_pt3	89.75	11.29	101.04	76.22	23.78
3223_b_pt4	89.60	10.94	100.54	76.75	23.25
3223_a_pt1	89.49	10.47	99.96	77.51	22.49
3223_a_pt2	89.19	11.03	100.22	76.52	23.48
3223_a_pt3	89.62	10.08	99.70	78.18	21.83
3223_a_pt4	89.25	11.01	100.26	76.56	23.44
3223_a_pt5	89.06	11.19	100.25	76.24	23.76
3223_a_pt6	89.10	10.94	100.04	76.65	23.35
3223_a_pt7	89.70	10.48	100.18	77.53	22.47
3223_a_pt8	89.11	11.22	100.33	76.19	23.81
3223_a_pt9	89.25	10.88	100.13	76.77	23.23
3223_a_pt10	89.32	10.96	100.28	76.65	23.35
3223_a_pt11	89.22	11.08	100.30	76.45	23.55
322.2 U-10Mo					
3222_a_pt02	89.18	10.93	100.11	76.68	23.32
3222_a_pt01	88.86	11.37	100.23	75.91	24.09
3222_a_pt03	89.14	11.29	100.43	76.09	23.91
3222_a_pt04	89.27	11.37	100.64	75.98	24.02
321.2 U-7Mo					
3212_b_pt1	93.02	7.87	100.89	82.66	17.34
3212_b_pt2	92.41	8.00	100.41	82.31	17.69
3212_b_pt3	93.06	7.92	100.98	82.57	17.43
3212_b_pt4	93.14	7.75	100.89	82.89	17.11
323.3 U-13Mo					
3233_a_pt1	86.36	14.13	100.49	71.13	28.87
3233_a_pt2	86.47	14.30	100.78	70.90	29.10
323.4 U-13Mo					
3234_a_pt1	86.96	14.33	101.29	70.98	29.02
3234_a_pt2	86.85	14.46	101.31	70.77	29.23
3234_a_pt3	86.70	14.46	101.16	70.73	29.27
3234_b_pt4	86.82	14.41	101.23	70.84	29.16
3234_b_pt5	87.00	14.36	101.36	70.95	29.05

APPENDIX C

X-RAY DIFFRACTION SPECTRA

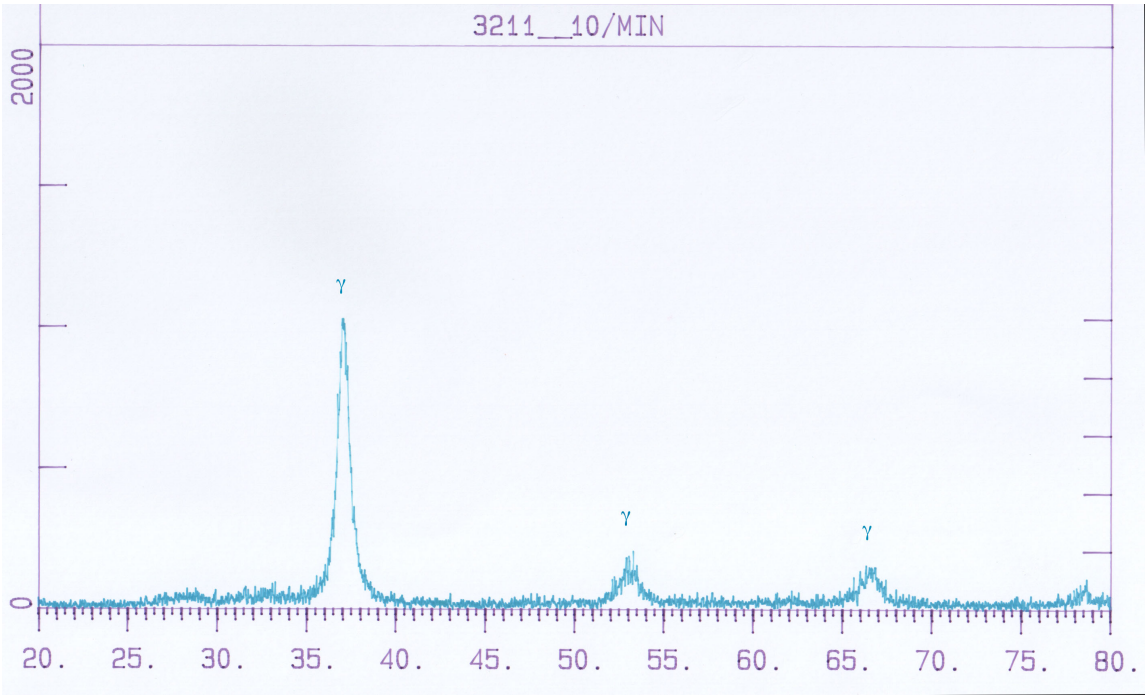

Figure C-1: Gamma stabilized U-7Mo alloy

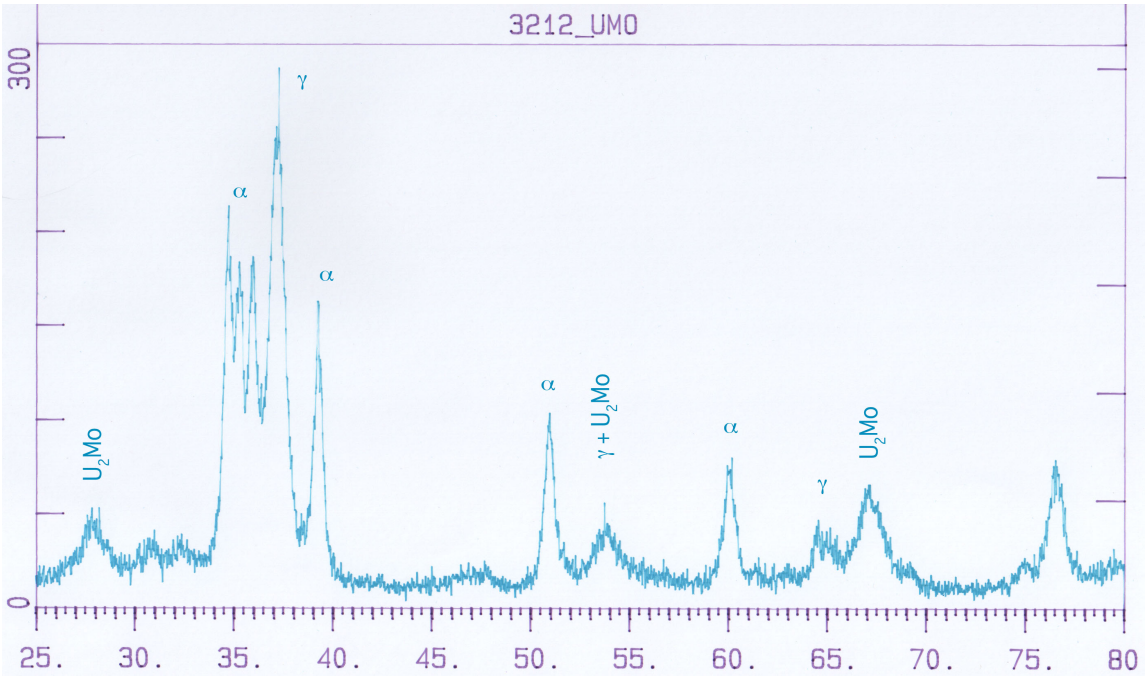

Figure C-2: Gamma decayed U-7Mo alloy (96 hours at 500 C).

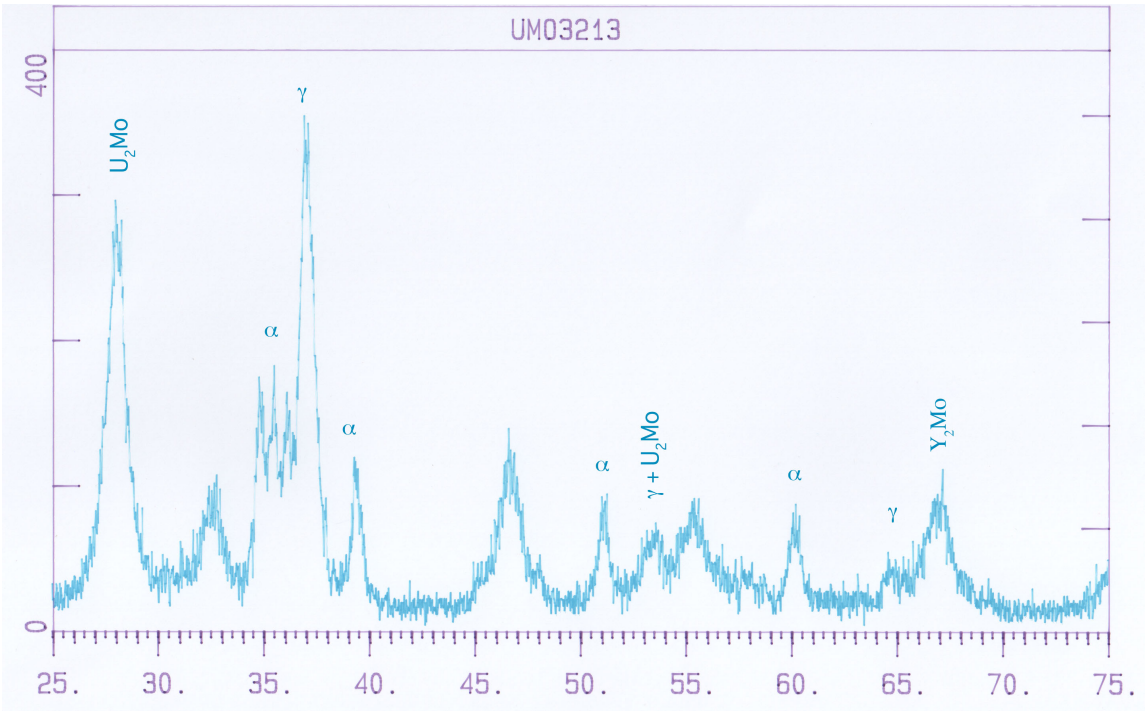

Figure C-3: Partially gamma decomposed U-7Mo (5 hours at 500 C).

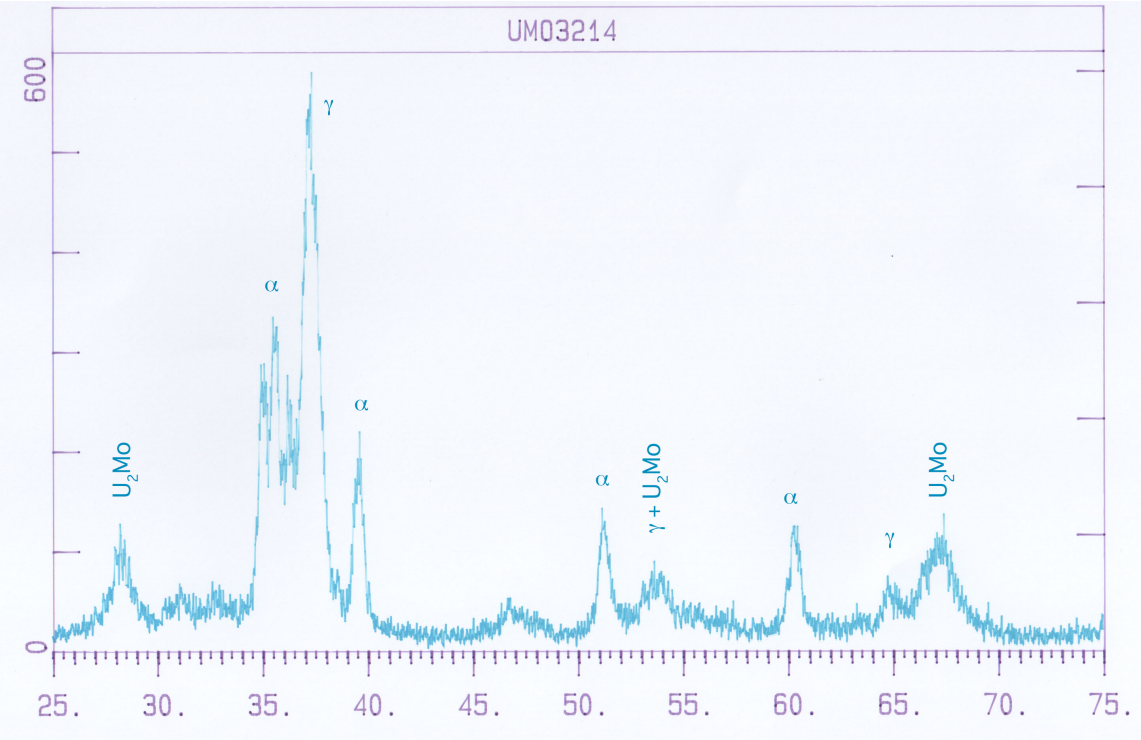

Figure C-4: Partially gamma decomposed U-7Mo (14 hours at 500 C).

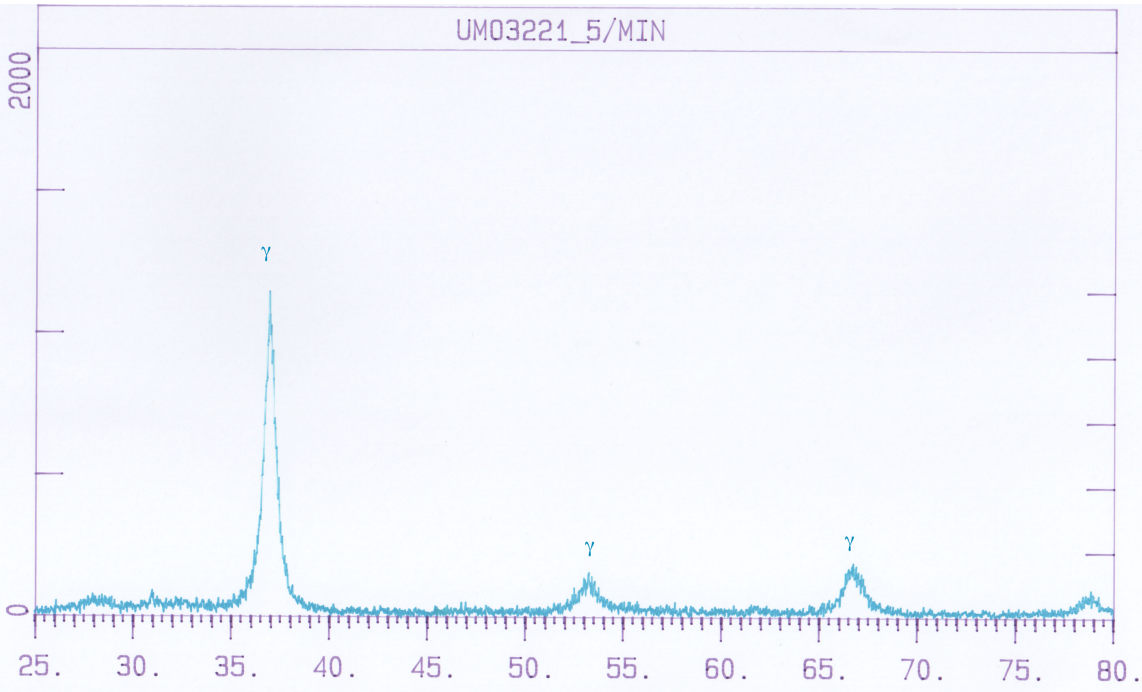

Figure C-5: Gamma stabilized U-10Mo.

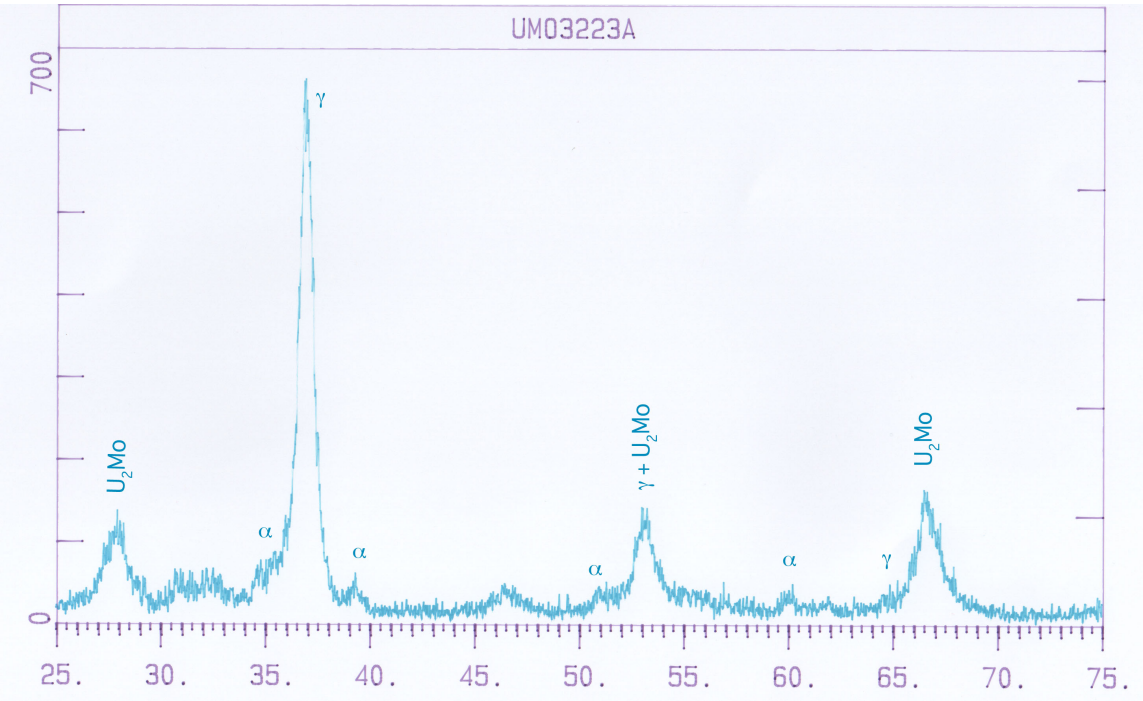

Figure C-6: Partially gamma decomposed U-10Mo (40 hours at 500 C).

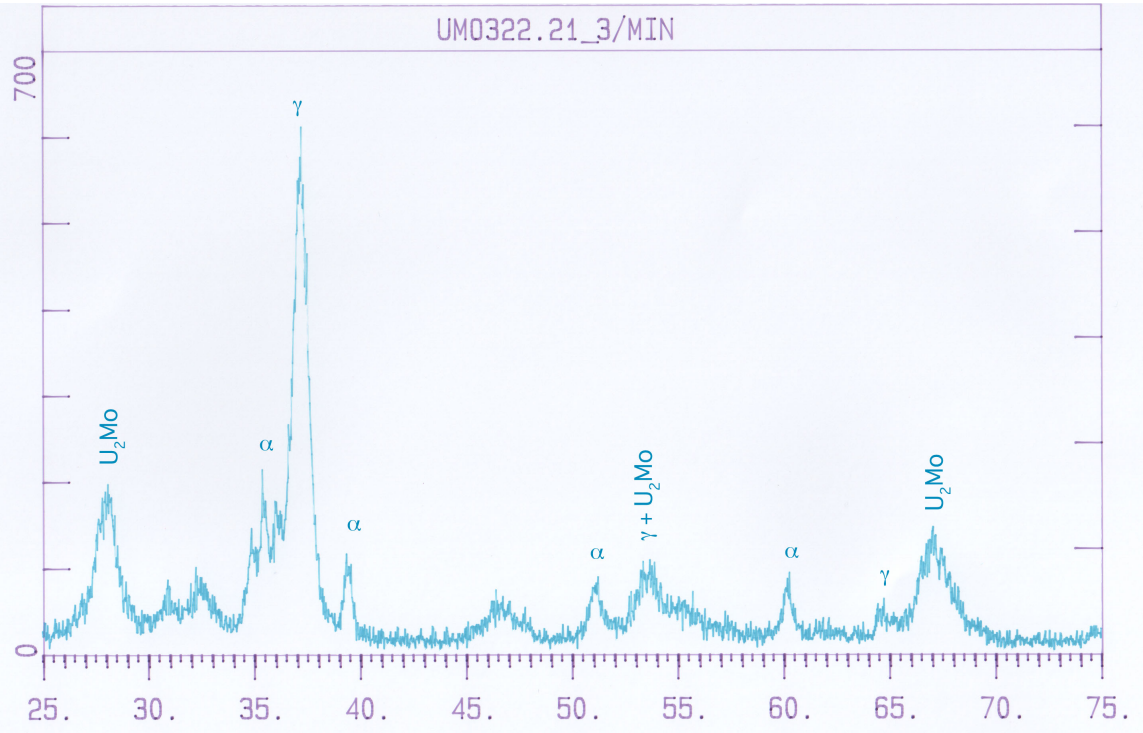

Figure C-7: Partially gamma decomposed U-10Mo (96 hours at 500 C).

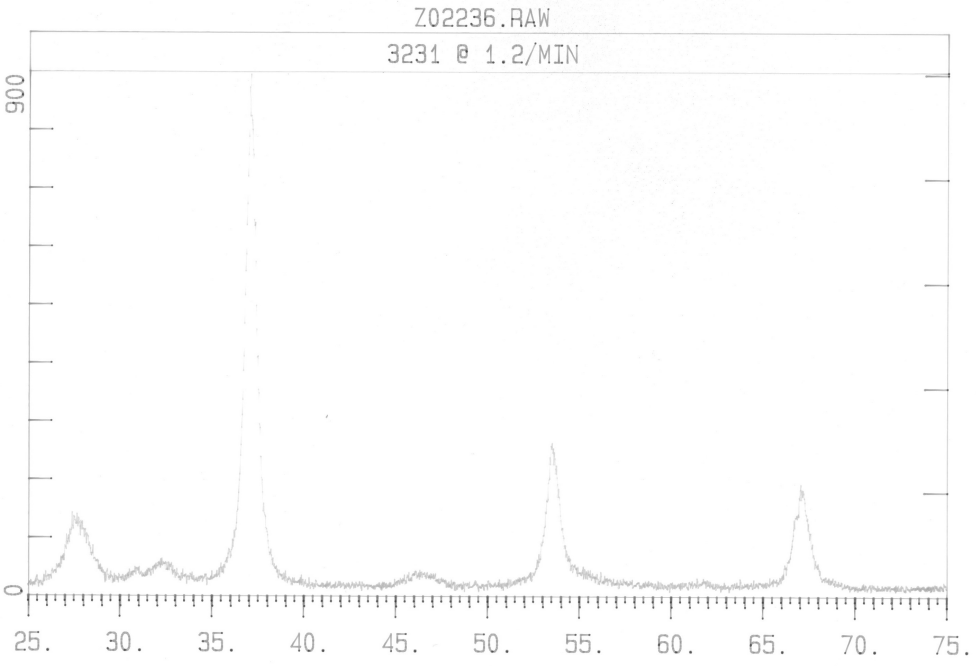

Figure C-8: Partially decomposed U-13Mo (96 hours at 500 C)

APPENDIX D

USEFUL EQUATIONS AND TABLES

The conversion from atom percent to weight percent is given by the following equation:

$$wt\%(x) = {}^{w}\!/_{0}(x) = A(x)\cdot at\%(x)\cdot \frac{100}{A(x)\cdot at\%(x) + A(y)\cdot at\%(y)}$$

Melting Point Equations

The melting point of uranium and molybdenum are 1132.15C and 2617C, respectively. The melting point of alloys of the two metals range between these two temperatures, although for wt% Mo ranges of 0 to 15% the melting point ranges from 1132 C to 1200 C.

"The solidus line for the U-Mo alloy for the range of the Mo content $0 \le x_{Mo} \le 4\ at\%$ from the U-Mo phase diagram[13] is used to obtain an equation for U-Mo melting temperature given below. It is valid up to approximately 13 wt% molybdenum. "

$$T_m = 1.408\times 10^3 - 2.912\, x_{Mo} + 0.1606\, x_{Mo}{}^2$$

where x_{Mo} is the Mo content in the U-Mo alloy in atom %, and T_m is in K.

Table D-1: Melting point of U-Mo alloys.

Alloy wt % Mo	Predicted	Measured[28]
	C	C
0	1135.0	1135
2	1124.5	1135
5	1122.8	1135
6.5	1127.1	1135
8	1134.1	1135
9	1140.3	1160

USEFUL TABLES

Table D-2: Thermal conductivity data for U-Mo alloys[13].

Comp. (wt.%)	Temp. (°C)	Thermal Conductivity ($W \cdot m^{-1}K^{-1}$)	Reference
U-5Mo	127 177 227 277 327 377 427 477 527	22.1 22.8 23.5 24.2 24.9 25.6 26.9 28.2 29.5	[15,20]
U-8Mo	10-100	14.2	[14]
U-9Mo	100	16.7	[11]
	200	20.9	
	300	26.8	
	400	32.6	
	500	38.5	
U-9.2Mo	20 100 200 300 400 500 600	14.3 16.6 19.4 22.3 25.1 27.9 31.1	[17]

Table D-2 continued.

Comp. (wt. %)	Temp. (°C)	Thermal Conductivity ($W \cdot m^{-1}K^{-1}$)	Reference
U-10Mo	23 100	12.1 14.2	[12]
	200	14.2	
	300	17.2	
	400	20.1	
	500	23.0	
	600	26.4	
	700	30.1	
	800	33.9	
	1000	37.7	
U-10Mo	25	9.7, 9.0	[13]
	100	11.7, 10.4	
	200	14, 12.6	
	300	17.2, 15.4	
	400	21.6, 19.3	
	500	25.7, 23.2	
U-10Mo	20 100 200 300 400 500 600	12.1 13.8 17.3 20.1 23.3 27.2 30.1	[15]
U-10.7Mo	20 100 200 300 400 500 600	11.9 14.4 17.5 20.6 23.7 26.9 29.9	[18]
U-12Mo	10-100	13.8	[14]

VITA

Name:	John Thomas Creasy
Address:	Department of Nuclear Engineering, Texas A&M University, MS 3133, College Station TX 77845
Email Address:	johncreasy@gmail.com
Education:	B.S., Nuclear Engineering, Texas A&M University, 2006 M.S., Nuclear Engineering, Texas A&M University, 2011